Scale Adaptive Turbulence Modeling for in-Vessel Sodium Thermal Hydraulics

By

Michael Acton

B.S. Nuclear Engineering, 2014
Missouri University of Science and Technology

SUBMITTED TO THE DEPARTMENT OF NUCLEAR SCIENCE AND ENGINEERING
IN PARTIAL FULFILLMENT OF THE REQUIREMENTS FOR THE DEGREE OF

MASTER OF SCIENCE IN NUCLEAR SCIENCE AND ENGINEERING
AT THE
MASSACHUSETTS INSTITUTE OF TECHNOLOGY

JUNE 2016

Signature of Author:_____
Michael Acton
Department of Nuclear Science and Engineering
May 20, 2016

Certified by _____
Emilio Baglietto, PhD
Norman C. Rasmussen Associate Professor of Nuclear Science and Engineering
Thesis Supervisor

Certified by _____
Neil Todreas, ScD
KEPCO Professor of Nuclear Science and Engineering, Emeritus
Thesis Reader

Accepted by _____
Ju Li, PhD
Battelle Energy Alliance Professor of Nuclear Science and Engineering
Chairman, Department Committee for Graduate Students

Scale Adaptive Turbulence Modeling for in-Vessel Sodium Thermal Hydraulics

By

Michael Acton

Submitted to the Department of Nuclear Science and Engineering on
May 20, 2016
in Partial Fulfillment of the Requirements for the Degree of

MASTER OF SCIENCE
IN NUCLEAR SCIENCE AND ENGINEERING

Abstract

Computational fluid dynamics is a powerful tool for the simulation of nuclear reactor coolant flows, such as in sodium fast reactors. In these reactors, the phenomenon of thermal striping – characterized by oscillatory turbulent mixing of non-isothermal coolant flows – has the potential to damage the structural integrity of reactor instrumentation and structural materials. At present, large eddy simulation is the only turbulence modeling approach which can sufficiently resolve and predict the mixing behavior of thermal striping, including temperature fluctuation and fluctuation frequencies. The extreme computational cost requirements of large eddy simulation application preclude the use of CFD for large engineering applications. In this work, the performance of the newly developed STRUCT hybrid turbulence model (Lenci, 2016) is evaluated on three representative test cases in comparison to traditional unsteady Reynolds-Averaged Navier-Stokes (URANS) and large eddy simulation (LES) models. Results indicate excellent potential for application of the STRUCT approach to sodium thermal striping flows. Best practice guidelines are developed and discussed.

Thesis Supervisor: Emilio Baglietto
Title: Norman C. Rasmussen Associate Professor of Nuclear Science and Engineering

Thesis Reader: Neil Todreas
Title: KEPCO Professor of Nuclear Science and Engineering, Emeritus

Acknowledgments

I am indebted to my research advisor, Professor Baglietto who offered invaluable guidance and support to me in this work. He served as a great teacher to me and whose years of experience I was very fortunate to learn from. He also developed the Cubic k-ε model and helped create the STRUCT model, both of which were critical to this research. I am also deeply indebted to fellow graduate student Giancarlo Lenci, whose development of the STRUCT model was critical to this research. Furthermore, he was a patient and helpful teacher from whom I learned much about CFD and turbulence. I would like to acknowledge fellow graduate students Etienne DeMarly and Benjamin Magolan for their contribution to the research devoted to grid-to-rod-fretting. In addition, I would like to thank my fellow CFD team members for their helpful advice and comments of this research. Finally, I would like to thank TerraPower for their support, without whom this work would not be possible.

Table of Contents

List of Figures

List of Tables

Nomenclature

Acronyms

ANL	Argonne National Laboratory
BCD	Bounded Central Differencing
CRIEPI	Central Research Institute of Electric Power Industry
CEA	Commissariat à l'énergie atomique et aux énergies alternatives
CFD	Computational Fluid Dynamics
DES	Detached Eddy Simulation
DNS	Direct Numerical Simulation
GFR	Gas cooled Fast Reactor
GTRF	Grid-to-Rod-Fretting
JAEA	Japan Atomic Energy Agency
KAERI	Korea Atomic Energy Research Institute
LES	Large Eddy Simulation
LDA	Laser Doppler Anemonetry
LSQ	Least Squares
LMFBR	Liquid Metal Fast Breeder Reactor
LRSFM	Low Reynolds Stress and Heat Flux
NLEVM	Non-Linear Eddy Viscosity Model
PANS	Partially Averaged Navier-Stokes
PIV	Particle Image Velocimetry
PWR	Pressurized Water Reactor
RNG	Re-Normalization Group
RANS	Reynolds-Averaged Navier-Stokes
RSM	Reynolds Stress Model
RMS	Root Mean Square
SAS	Scale Adaptive Simulation
SST	Shear Stress Transport
SFR	Sodium Fast Reactor
SGS	Sub-Grid Scale
UDV	Ultrasound Doppler Velocimetry
URANS	Unsteady Reynolds-Averaged Navier-Stokes
WALE	Wall Adapting Local Eddy

Mathematical and Greek Characters

Notation	Units	Description
ρ	kg m^{-3}	Density
∇	—	Del Operator
U	m s^{-1}	Velocity
v	m s^{-1}	Velocity
μ	Pa s	Molecular Viscosity
μ_t	Pa s	Eddy Viscosity
ν	kg m^{-3}	Kinematic Viscosity
∇^2	m^2 s^{-1}	Laplacian
f	s^{-1}	Frequency
f_r	s^{-1}	STRUCT controlled frequency parameter
P	Pa	Pressure
c_p	J K^{-1}	Specific Heat Capacity
T	K	Temperature
q''	W m^{-2}	Heat Flux
q'''	W m^{-3}	Volumetric Heat Source
ϕ	—	STRUCT controlled eddy viscosity reduction parameter
Re	—	Reynolds Number
L	m	Length Scale
η	m	Kolmogorov Length Scale
ε	J kg^{-1} s^{-1}	Turbulent Kinetic Energy Dissipation Rate
y^+	—	Dimensionless Wall Distance
k	J kg^{-1}	Turbulent Kinetic Energy
δ_{ij}	—	Kronecker Delta
S_{ij}	s^{-1}	Strain Rate Tensor
τ_{ij}	J kg^{-1}	Reynolds or Residual Stress Tensor
Ω_{ij}	s^{-1}	Rotation Rate Tensor
Δ	m	Filter Size for LES models
$\bar{II}$	s^{-2}	Second Invariant for Velocity Gradient Tensor
ω	s^{-1}	Specific Dissipation Rate

1   Introduction

Understanding the fluid flow behavior in nuclear reactors is critical for the prediction of coolant distribution and heat transfer characteristics. Traditional analysis uses lumped-parameter system codes wherein the average coolant properties in a large control volume is calculated. However, this approach is not applicable for situations where complex three-dimensional effects are important or where turbulence is critical to the flow understanding. In these situations, computational fluid dynamics (CFD) codes which solve the discretized Navier-Stokes equations in three dimensions with additional turbulence modeling can become a necessary tool.

Many different turbulence modeling approaches are available which vary in terms of flow description and computational cost. For many industrial flows, relatively low cost, steady state Reynolds Average Navier-Stokes (RANS) or (U)nsteady RANS models are the only tractable approaches, and even URANS models can soon become burdensome with current computational resources. Unfortunately, the modeling assumptions of RANS models, which allows them to be solved on coarse computational meshes, also renders them insensitive to fine scale details of turbulence, making them invalid on more complex, rapidly varying flow conditions. Furthermore, the limited degree of flow description renders RANS models incapable of accurately predicting fluctuating flow field parameters even for simpler applications.

One such challenging application is thermal striping in sodium fast reactor (SFR) flows. Thermal striping is the attenuation of fluctuating temperature fields by structural materials leading to fatigue and failure. These fluctuating temperature fields are caused by turbulent non-isothermal coolant streams mixing in a large plenum.

Since RANS models are of limited applicability for complex mixing features typical of SFRs, large eddy simulation (LES) models are leveraged for their increased level of flow description. Unfortunately, LES models require computational resources orders of magnitude greater than URANS models – often making the simulation impractical for engineering applications.

Due to the large gap between LES and URANS models in terms of cost and accuracy a large class of 'hybrid' turbulence models have been proposed, which seek to balance the accuracy of LES with the low cost and robustness of URANS. Hybrid models however have not yet achieved widespread industrial application, due to the lack of general applicability on most engineering flow cases. When tested outside of their verified applicability space, hybrid models often perform worse than the URANS models they seek to improve.

In this thesis, the performance of the recently developed STRUCT hybrid turbulence model of Lenci (2016) is evaluated on thermal striping flows relevant to sodium fast reactors. Furthermore, the model is assessed on a test case for a pressurized water reactor (PWR) assembly flow, which has been selected due to the similarity of turbulence modeling challenges to that of thermal striping flow cases. The STRUCT turbulence model has been developed for industrial use, aiming to achieve results always better than or equal to those generated by URANS models. Successful application of the STRUCT

turbulence model for thermal striping flow conditions would enable the use of CFD for engineering design of SFR flow cases, reducing the likelihood of thermal striping induced failure in future SFRs.

1.1   Objectives

The objective of this work is to evaluate the performance of the STRUCT turbulence model in simulating thermal striping flows. The work will be performed as follows:

1. Selection of appropriate test cases
2. Evaluate the performance of the STRUCT model on each test case
3. Determine simulation guidelines for simulating thermal striping using STRUCT and other models

1.2   Structure

The thesis is divided into seven chapters, using the general logic of selection and then description of each test case followed by evaluation of modeling approaches on each case. The remaining chapters are outlined as follows:

Chapter 2 highlights the engineering challenge of thermal striping and discusses a complete literature review of the subject, including past experimental and numerical work.

Chapter 3 introduces computational fluid dynamics and turbulence modeling. It discusses the theoretical and mathematical approach to turbulence and introduces the turbulence modeling approaches used in this work including that of the STRUCT approach.

Chapter 4 discusses the Japanese Atomic Energy Agency (JAEA) triple jet test, providing a review of previous work as well as new results shown for this work with application of the STRUCT model.

Chapter 5 discusses the PWR test case, reviewing previous PWR assembly work and showing the performance of the STRUCT model in matching experimental predictions. Particular emphasis on turbulent coherent structures is made in this section.

Chapter 6 provides a description of the Argonne National Laboratory (ANL) MAX facility test case as well as discussing STRUCT results in comparison to experiment and in extrapolation outside of experimental bounds.

Chapter 7 concludes the thesis, providing a summary of the work performed with STRUCT and other turbulence models.

2 Thermal Striping

2.1 Phenomena and Challenges

Thermal striping can arise when turbulent coolant streams of different temperatures mix in the vicinity of sensitive structural materials. The temperature fluctuations are attenuated by structural materials causing thermal fatigue induced failures. In light water reactors (LWR) this typically occurs in mixing T-Junctions and has been responsible for failures at the Japanese PWR Tomari-2 and the French PWR Civaux (Peniguel et al, 2003). The T-Junction is a well-studied experimental configuration for turbulent mixing ((Lee et al., 2009, Hu and Kazimi, 2006, Kawamura et al., 2002, Yuki et al., 2006). The geometry of a prototypical mixing junction in LWRs is shown in Figure 2.1.1.
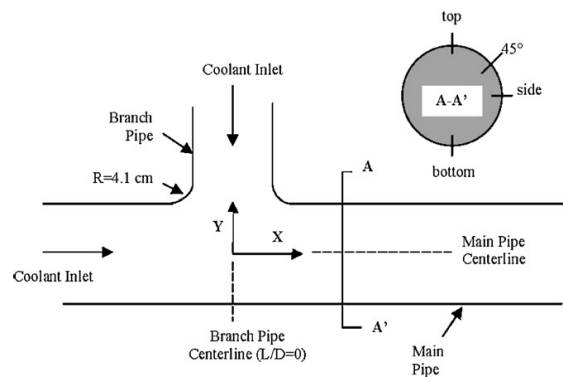
Figure 2.1.1 Typical configuration of T-junction mixing experiment. Taken from (Lee et al., 2009)

Thermal striping in the upper plenum of an SFR is of particular concern, where the hot coolant flowing from the core sub-assemblies could cause damage to upper plenum instrumentation and materials. Failure of such components can remove reactors from service for extended periods of time, demanding costly repairs. This has been reported for both the Phenix and Superphenix SFRs (Gelineau and Sperandio, 1994). The accurate prediction of thermal striping, therefore, is of utmost design and operations importance. A typical configuration of the upper plenum in a SFR is shown in Figure 2.1.2.
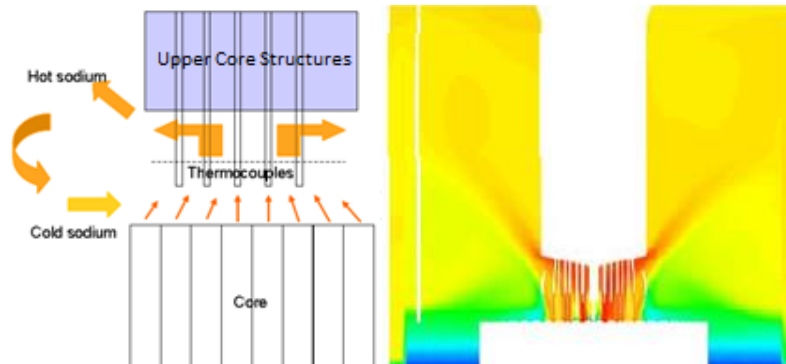
Figure 2.1.2 Typical configuration of the upper plenum region in a pool type (left: taken from (IAEA, 2006)) and loop type SFR (right: taken from (Ohira et al., 2013))

2.2 Past Experimental and Numerical Work

The evolution of thermal striping experimental work has moved from low resolution large scale experiments to small high resolution experiments, suitable for analysis with modern CFD codes. The experiments in this section are categorized by geometrical arrangement.

2.2.1 Parallel Triple Jet

The parallel triple jet geometry consists of three non-isothermal inlet jets of fluid mixing in an open geometry. This configuration is simple and symmetric, leading to easy experimentation and simulation. A downside of this geometry is the tendency of the two hotter jets to "insulate" the mixing process from extreme instability – a situation not necessarily shared with SFR conditions.
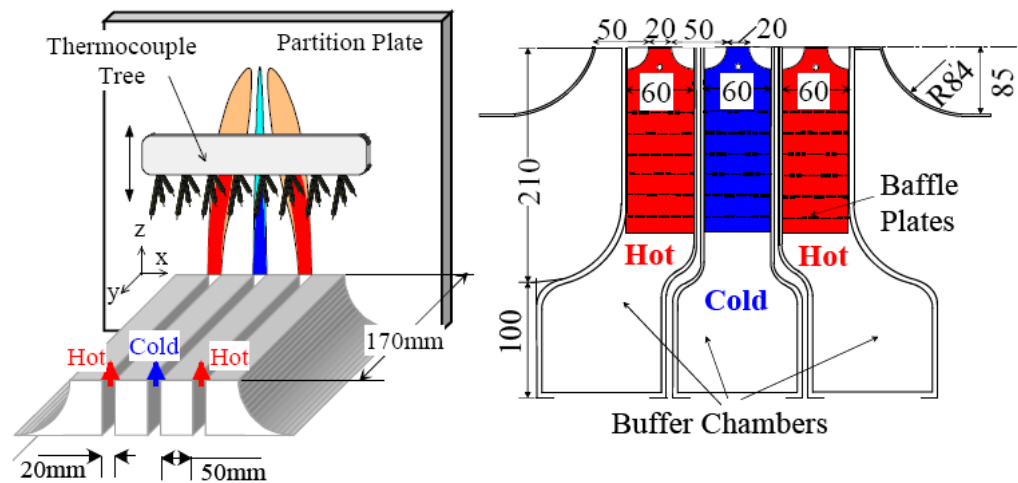
Figure 2.2.1 JAEA triple jet experiment testing geometry showing the inlet valves, thermocouple tree, and partitioning plate. Taken from (Kimura et al., 2007a)

The parallel triple jet experimental geometry was first experimentally studied by Tokuhiro and Kimura (1999) at the JAEA. This configuration is depicted in Figure 2.2.1 JAEA triple jet experiment testing geometry showing the inlet valves, thermocouple tree, and partitioning plate. Taken from (Kimura et al., 2007a) The mean and fluctuating temperature profiles at different experimental elevations are shown in Figure 2.2.2.
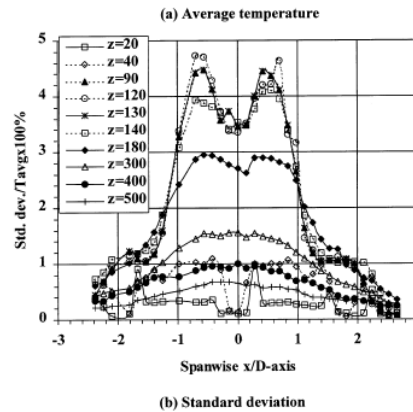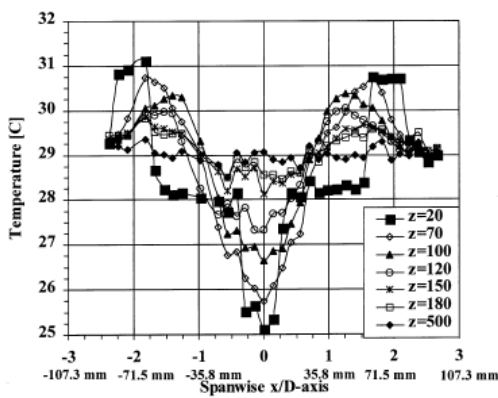
Figure 2.2.2 Mean (left) and RMS (center) temperature profiles in the JAEA triple experiment, as well as instantaneous temperature image (right). Taken from (Tokuhiro and Kimura, 1999)

Simulation of the experiment has been investigated by many authors. Nishimura et al. (2000) simulated the experimental geometry with the standard k-ε turbulence model and the Low Reynolds Stress and Heat Flux (LRSFM) second moment closure model. This work showed the limitation of URANS turbulence models for calculating accurately the mixing phenomena between the jets. The LRSFM model showed improvement by accurately predicting fluctuation frequencies, while still failing to predict the temperature profiles in the regions of strong mixing. These conclusions were confirmed by Nishimura and Kimura (2003), Kimura et al. (1999) and Nishimura et al. (2000) with the latter showing strong improvement in mixing predictions using no turbulence closure.

The sodium thermal striping heat transfer characteristics were studied by Kimura et al. (2007b) who created an empirical relation for the sodium heat transfer coefficient in thermal striping flows. Kimura et al. (2007a) evaluated a similar heat transfer function using LES which was found to accurately predict all quantities of interest in the mixing regions. Further study by Jung and Yoo, (2004) and Cao et al. (2012a) and Chaco et al. (2011) has confirmed the suitability of LES for the parallel triple jet geometry.

A similar experiment was conducted by the Korea Atomic Energy Research Institute (KAERI, 2006) using air as the working fluid against which Choi and Kim tested the two-layer k-ω, k-ω SST, and V2-f turbulence models. The authors confirmed the difficulty of using URANS turbulence models for predicting thermal striping mixing, while recommending the k-ω SST model for providing the closest match to experiment.
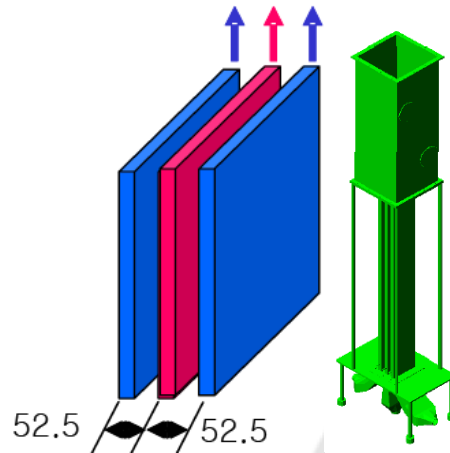
Figure 2.2.3 KAERI triple jet experimental geometry. Taken from (KAERI, 2006)

2.2.2   Coaxial Jet

The coaxial jet geometry simulates the flow around a control rod, where cold fluid is surrounded by hot fluid from nearby fuel rod channels. A prototypical example of the coaxial jet configuration is shown in Figure 2.2.4.
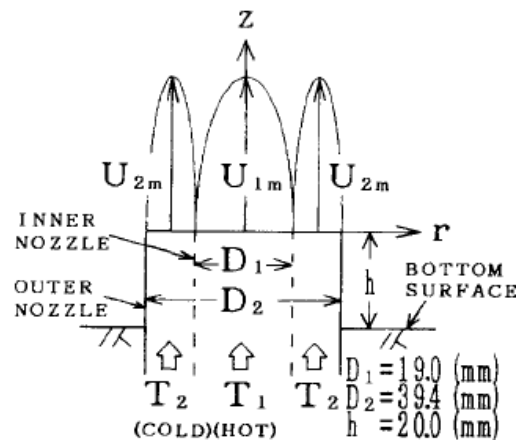
Figure 2.2.4 Prototypical description of the coaxial configuration. Taken from (Ushijima et al., 1990)

This geometry was the focus of numerous early experimental works by the Tokyo University of Science (Hattori et al., 1998), CEA and KAERI (Tenchine and Moro, 1997), and CRIEPI (Moriya and Ohshima, 1990).

Hattori et al. (1998) analyzed the experimental effect of annulus jet velocity ratios on velocity and turbulence intensity concluding that temperature fluctuations are most severe at equivalent jet velocities. Moriya and Ohshima (1990) determined the effect of the Reynolds and Peclet number on the temperature fluctuations, frequencies, and temperature profiles.

Ushijima et al. (1990) analyzed the same experimental setup with the RSM of Launder et al. (1975), showing relatively strong performance in predicting temperature and fluctuation profiles but with some limitation in the prediction of heat fluxes. Tenchine and Nam (1987) showed that the standard k-ε incorrectly predicts mixing at low elevations; while Tenchine and Moro (1997) showed significant improvements with LES.

This geometry has been most recently studied experimentally by Lu et al. (2012) and has been designed for study with CFD. Xiang-bin et al. (2012) used LES to study the temperature fluctuation distribution for application to PWR upper plenums, while Cao et al. (2012b) extended this work by analyzing the effect of inlet velocity ratios.

2.2.3   Twin-Jet

The twin jet geometry is a simple geometry of two non-isothermal jets mixing in an open geometry. However, due to its non-symmetric temperature configuration, the twin jet configuration may be the most suited for measuring the instabilities of jet mixing that would be characteristic of the thermal striping phenomena in actual SFRs. The typical twin-jet geometry is shown in Figure 2.2.5.
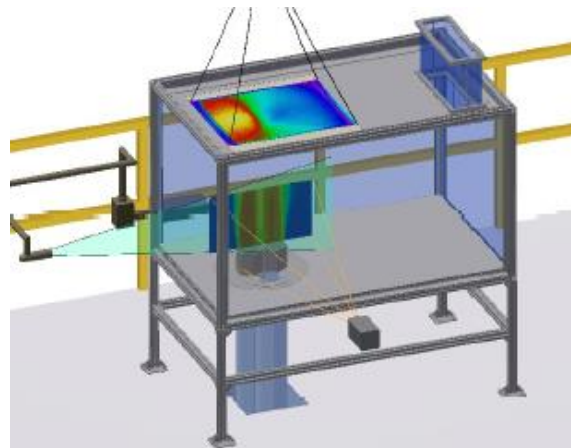
Figure 2.2.5 Twin-jet configuration with hexagonal inlets. Taken from (Lomperski et al., 2012)

Brunings (1982) utilized the first experimental work for thermal striping with a simplified version of the twin jet geometry; the work was primarily concerned with qualitatively determining the severity of potential thermal striping in an SFR.

Wakamatsu (1995) analyzed through a separate experiment at CRIEPI the effect of the vertical distance between the jets and the material on the temperature and velocity fields, as well as on the attenuation of temperature in the material itself.

The twin jet geometry was recently experimentally studied by Crosskey and Ruggles (2014) and Carasik et al. (2014) and Wang et al. (2016) at the University of Tennessee Knoxville along with researchers at Texas A&M University. The analysis consisted of LDA measurements of the flow field of two

isothermal jets in a mixing tank and used wavelet analysis to determine the effect of eddy size in the flow.

Omotowa et al. (2012) analyzed the twin-jet geometry using the standard k-ɛ and RNG k-ɛ turbulence models to determine the effect of jet spacing and velocity ratios on the mixing and merger of the jets.

Finally, the twin jet Argonne National Laboratory MAX facility (Lomperski et al., 2012; Merzari et al., 2010; Pointer et al., 2009) has been constructed for high spatial and temporal resolution study of thermal striping with PIV measurements of the air working fluid. The experiment is still ongoing and as such all experimental data and analysis is in a preliminary stage.

2.2.4   *Scale Experiments*

Scale model sodium fast reactor tests utilize large mixing tanks and inlet jets that are related to SFR thermal-hydraulics through the equivalency of Reynolds and Peclet number. Due to the nature of the tests, the temperature and velocity measurements may not be fine enough for accurate use alongside CFD calculations.

Two significant scale experiment tests were undertaken by the CRIEPI and the JAEA. The CRIEPI scale experiment (Moriya et al., 1991) considered a seven-assembly water model to determine the effect of control rods and guide tubes on the location and magnitude of thermal striping, and made recommendations on ideal configurations. Kobayashi et al. (2014) studied a 1/3 scale water model of the proposed Japan Sodium Fast Reactor to experimentally determine the thermal striping fields in the reactor, and made design recommendations to mitigate the effect.

3 Computational Fluid Dynamics and Turbulence Modeling Background

In this section a brief introduction to computational fluid dynamics (CFD) and turbulence modeling will be given to the extent necessary to facilitate discussion of thermal striping and the understanding of the hybrid modeling approach adopted. The interested reader is directed to the standard textbook by Pope (2001) for a discussion of the mathematical modeling of turbulence; the textbook by Durbin and Reif (2011) for a discussion of the theory of turbulence modeling, and finally the textbook by Ferziger and Peric (2002) for a discussion of numerical implementation in CFD codes.

The behavior and properties of any continuum fluid can be described through conservation equations for mass, momentum, and energy which can be written as:

Mass:

$$\frac{\partial \rho}{\partial t} + \nabla \cdot (\rho U) = 0 \qquad\qquad 3.1$$

Momentum:

$$\rho \frac{\partial v}{\partial t} + \rho U \cdot \nabla U = -\nabla P + \mu \nabla^2 U + \rho f \qquad\qquad 3.2$$

Energy:

$$\rho c_p \left(\frac{dT}{dt} + U \cdot \nabla T \right) = -\nabla \cdot q'' + q''' + \phi \qquad\qquad 3.3$$

It is assumed that the fluid is a constant property Newtonian fluid. For simplicity the fluid is considered to be incompressible i.e. $\rho = 0$ rendering the mass equation as:

$$\nabla \cdot U = 0 \qquad\qquad 3.4$$

Together these equations are denoted as the Navier-Stokes equations and are generally accepted as sufficient to describe the behavior of a continuum fluid.

In computational fluid dynamics these equations are discretized and solved numerically either in finite element, finite volume, or finite difference form. The finite volume form is almost universally used in industrial CFD codes.

3.1 Turbulence

A fluid travelling at low kinetic energy is composed of fluid parcels travelling in a parallel streamline to other parcels, known as laminar flow. At high kinetic energy these fluid parcels shear from each other and travel in a pseudo-random turbulent streamline, enhancing mixing and decreasing momentum transport.
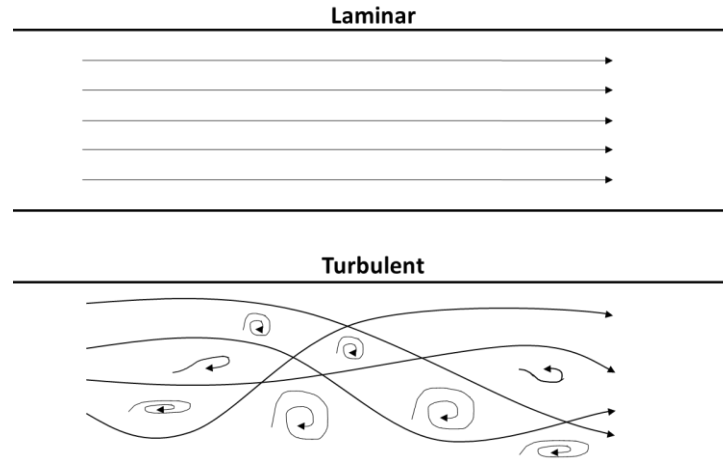
Figure 3.1.1 Example flow streamlines of laminar and turbulent flow in a pipe

The transition from laminar to turbulent flow is typically described in terms of the Reynolds number of the flow given by:

$$Re = \frac{\rho UL}{\mu} \qquad \qquad 3.5$$

Turbulence transition occurs between 3,000-5,000 while self-similar behavior occurs past 20,000.

Turbulent flows are characterized by eddies which are created by the shear of fluid parcels and are responsible for the chaotic nature of turbulent flows. These eddies range in size from the largest length scales on the order of the domain down to the smallest scales described as the Kolmogorov scale given by:

$$\eta = \left(\frac{\nu^3}{\varepsilon}\right)^{\frac{1}{4}} \qquad \qquad 3.6$$

Where ν is the kinematic viscosity, and ε is the dissipation of turbulent kinetic energy.

The energy of a turbulent flow was analyzed by Kolmogorov and classified into three distinct ranges: energy containing, inertial, and dissipation. In the energy containing range large eddies are created by velocity gradients in the flow, these eddies break down into smaller eddies in the inertial range, and

are finally dissipated due to molecular interactions in the dissipation range. The Kolmogorov scale describes this smallest scale of turbulent eddies.

In order to completely solve the Navier-Stokes equations, all scales – including the Kolmogorov scale – must be resolved. This is called Direct Numerical Simulation (DNS) and this requirement implies extreme computational cost due to the need for very fine spatial and temporal discretization. If DNS is attempted on a too coarse grid the effect of the small scale turbulence would be ignored, which introduces significant error to the solution.
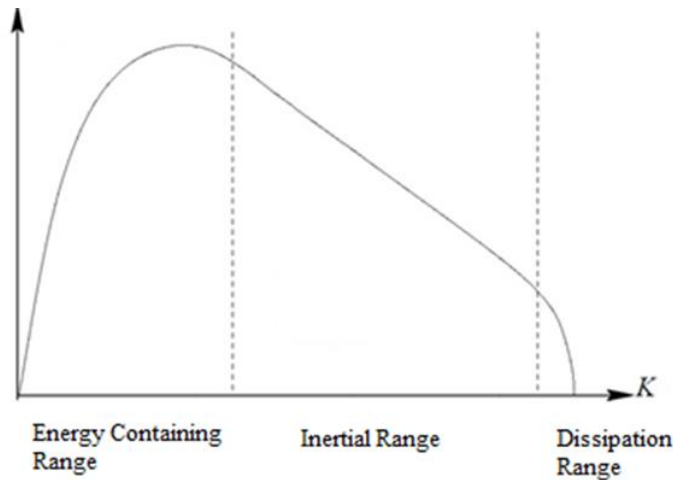
Figure 3.1.2 Turbulent cascade showing three distinct regions: energy containing, inertial, and dissipation ranges.

Instead, turbulence models attempt to solve the Navier-Stokes equations by introducing modeling assumptions to account for the effect of this small scale turbulence. There are two mainstream families of turbulence models which attempt this in different manners: Reynolds-Averaged Navier-Stokes (RANS) based models, and Large Eddy Simulation (LES) models.

3.2 Reynolds-Averaged Navier-Stokes

The foundation of RANS models is the decomposition of the instantaneous signal into a mean and a fluctuating component which is demonstrated for the velocity signal as:

$$U = \bar{U} + u' \qquad\qquad 3.7$$

This is graphically represented by Figure 3.2.1.
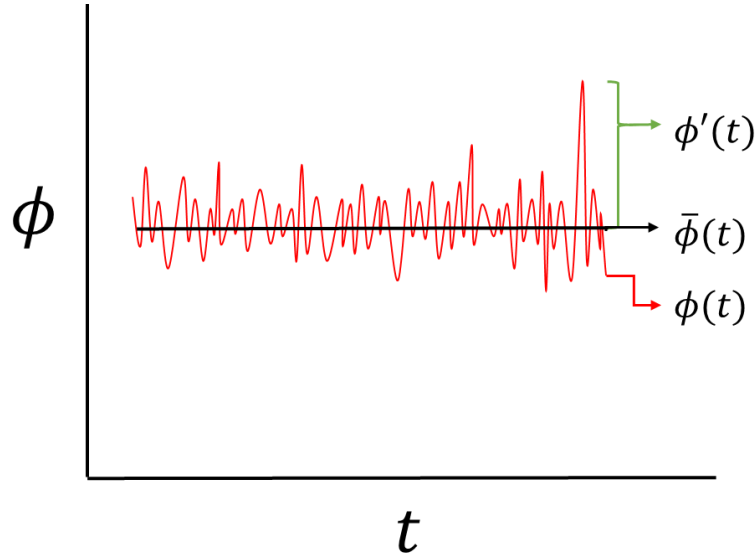
Figure 3.2.1 Decomposition of a steady state instantaneous signal into a mean and fluctuating component.

The Reynolds decomposition can also be viewed as an ensemble average over infinite flow representations plus an incoherent or random component. This is predicated on the concept of each flow solution as a single flow realization from many possible realizations. The Reynolds averaging operation is then applied to the Navier-Stokes equations generating the following RANS equation after arrangement:

$$\rho\frac{\partial \bar{U}}{\partial t} + \rho\bar{U}\cdot\nabla\bar{U} = -\nabla\bar{P} + \nabla(2\mu\boldsymbol{S} - \rho\overline{u_j'u_i'}) \qquad 3.8$$

Where **S** is the mean strain tensor given by:

$$S = \frac{1}{2}(\frac{\partial \bar{U}}{\partial x} + \frac{\partial \bar{U}}{\partial y}) \qquad 3.9$$

And $\rho\overline{u_j'u_i'}$ is termed the Reynolds stress tensor, and denoted by τ_{ij}

The Reynolds stress tensor is the only term in the RANS equation that is unclosed – but it is a symmetric tensor consisting of six unknown components. Two methods to solve the Reynolds Stress Tensor demarcate the two popular families of RANS models. Reynolds Stress Models (RSM), or second moment closures, directly attempt to solve each component of the tensor individually. These methods are not discussed in depth in this thesis – the interested reader is referred to chapter 11 of Pope (2001) for a more thorough discussion of RSMs. The second class of RANS models are termed eddy viscosity models and are discussed in the following section. Eddy viscosity models are the dominant class of models in industrial application.

The RANS equations can be implemented in a steady state or transient time advancement scheme. When implemented in transient mode – known as (U)nsteady RANS - a more appropriate theoretical decomposition of the instantaneous field is through the triple Reynolds decomposition.

$$U = \bar{U} + \hat{U} + u'$$ 3.10

Where $\hat{U}$ represents the time varying mean; while $\bar{U}$ remains the traditional time average. This decomposition is represented in Figure 3.2.2.
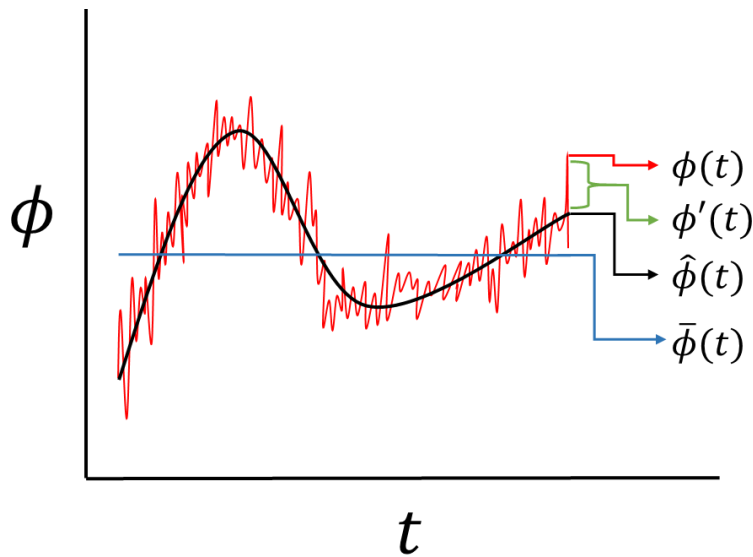
Figure 3.2.2 Triple decomposition of an unsteady instantaneous signal into mean, time varying mean, and fluctuating components

The RANS equations are a modelled form of the original Navier-Stokes equation – and as such almost all scales of motion are directly modelled (averaged); while the effect of turbulence on the flow is taken into account through the Reynolds Stress Tensor. This decomposition makes sense in many engineering applications because it is common to only require information regarding the effect of turbulence on mean flow quantities rather than directly capturing information on the turbulent flow field. However, this strategy also makes the RANS equations incomplete for understanding flows with emphasis on fluctuating quantities such as the fluctuating forces felt by nuclear fuel rods causing grid-to-rod-fretting.

A second limitation relates to the implicit assumption in the URANS decomposition that there is a separation of scales between mean and fluctuating quantities. This assumption is required to be true for the separation in the flow field performed in equation 3.10 between the time varying mean and the instantaneous fluctuations. This assumption does not hold for all engineering flows of interest, and this limitation will be discussed further in this thesis.

3.2.1   Eddy Viscosity Models

The most popular method for closing term τ_{ij} is through the Boussinesq approximation which relates the Reynolds Stresses to the mean strain rate through an "eddy viscosity" μ_t as in equation 3.11.

$$\tau_{ij} = \mu_t \left(\frac{\partial \bar{u}_i}{\partial x_j} + \frac{\partial \bar{u}_j}{\partial x_i} \right) \qquad\qquad 3.11$$

The eddy viscosity is also known as the turbulent viscosity and represents the assumed similarity between the effect of turbulence on the mean flow as the effect of molecular viscosity does.

Now τ_{ij} can be rewritten as:

$$\tau_{ij} = \frac{2}{3} k \delta_{ij} - 2\mu_t S_{ij} \qquad\qquad 3.12$$

Where k is the turbulent kinetic energy and is the trace of the Reynolds Stress Tensor.

Finally, the RANS equations with the eddy viscosity assumption can be considered identical to the instantaneous momentum equation except that the variables are now time-averaged and the molecular viscosity is increased with an added eddy viscosity. In this manner, it is apparent that the RANS equations with eddy viscosity assumption is equivalent to solving an increased viscosity fluid.

The assumption that the effect of turbulence is linearly proportional to and aligned with the mean strain rate has no rigorous experimental or theoretical root. The assumption of linear proportionality is a major limitation – which can be overcome through the use of higher order non-linear eddy viscosity models. These models will be described further in a separate subsection.

The assumption that turbulence behaves analogously to molecular viscosity is also a major limitation which will be explored further, and models such as RSM and LES that do not rely on the Boussinesq approximation are sometimes required. However, these approaches carry their own limitations which limit their widespread application. RSMs require the closure of six terms in the Reynold's Stress Tensor and as such, many additional modeling assumptions must be made as compared to eddy viscosity models. These additional assumptions often render RSMs less accurate than their simple eddy viscosity counterparts. LES on the other hand offer superior performance in most flow scenarios, but their extreme computational requirements limit their use. Due to the major limitations of RSMs and LES, simple eddy viscosity models still remain the dominant class of models in engineering applications.

After applying the eddy viscosity assumption, the only unclosed term in the RANS equation is the eddy viscosity itself – the method employed to solve this is the differentiation between different eddy viscosity RANS models.

3.2.2   Standard k-ε

The majority of eddy viscosity models compute the eddy viscosity as the product of a length and a velocity scale. A famous example of this is Prandtl's mixing length model which calculates it as the product of mixing length squared and the mean shear rate.

The most popular turbulence models currently in use are based on this concept of length and velocity scales, but calculate these scales through the introduction of additional transport equations for quantities – enabling non-local effects to be calculated locally. The work in this thesis focuses on so called two-equation k-ε models that introduce transport equations for the turbulent kinetic energy (k) and turbulent dissipation rate (ε).

The transport equation for k is as follows:

$$\frac{\partial k}{\partial t} + \bar{u}_j \frac{\partial k}{\partial x_j} = \frac{\partial}{\partial x_j}\left[(\mu + \frac{\mu_t}{\sigma_k})\right] + P_k - \varepsilon \tag{3.13}$$

The transport equation for ε is as follows:

$$\frac{\partial \varepsilon}{\partial t} + \bar{u}_j \frac{\partial \varepsilon}{\partial x_j} = \frac{\partial}{\partial x_j}\left[(\mu + \frac{\mu_t}{\sigma_\varepsilon})\frac{\partial \varepsilon}{\partial x_j}\right] + C_{\varepsilon 1}\frac{\varepsilon}{k}P_k - C_{\varepsilon 2}\frac{\varepsilon^2}{k} \tag{3.14}$$

The production term P_k is as follows:

$$P_k = 2\mu_t \bar{S}_{ij}\bar{S}_{ij} \tag{3.15}$$

The transport equations take the general form of a transport equation exhibiting convective transport, diffusion, production and destruction terms.

Finally, the eddy viscosity is solved as:

$$\mu_t = C_\mu \frac{k^2}{\varepsilon} \tag{3.16}$$

The standard k-ε model uses the coefficients from Launder and Spalding (1974) as $C_\mu = 0.09$, $C_{\varepsilon 1} = 1.44$, $C_{\varepsilon 2} = 1.92$, $\sigma_k = 1.0$, $\sigma_\varepsilon = 1.3$.

The standard k-ε model is one of the most commonly used turbulence models in engineering flows, and although it struggles in complex flow geometries, its performance is widely documented and

understood on a vast number of flow cases. These limitations are closely related to the linear relation implying isotropy of the Reynolds stresses as well as the intrinsic limitations of the URANS decomposition for rapidly varying flows and the eddy viscosity assumption's inherent limitation. Due to its widespread use in engineering flows, the standard k-ε model is selected as a baseline model for testing in this thesis.

3.2.3   Realizable k-ε

Observations of the standard k-ε model revealed that under adverse flow conditions, the standard k-ε model sometimes exhibits non-physical negative normal Reynolds stresses. The realizable k-ε (Shih et al., 1995) is a popular alternative to the standard k-ε that builds upon the former by imposing realizability (i.e. positivity enforcing) under all flow conditions. This is done through an alternate formulation for C_μ as follows:

$$C_\mu = \frac{1}{A_0 + A_s \frac{kU^*}{\varepsilon}}$$

3.17

Where U^* is provided as:

$$U^* = \sqrt{\bar{S}_{ij}\bar{S}_{ij} + \bar{\Omega}_{ij}\bar{\Omega}_{ij}}$$

3.18

And

$$A_0 = 4$$

3.19

$$A_s = \sqrt{6}cos\left(\frac{1}{3}acos\left(\sqrt{6}\bar{S}_{ij}\bar{S}_{jk}\bar{S}_{ki}\left(\bar{S}_{ij}\bar{S}_{ij}\right)^{-\frac{1}{3}}\right)\right)$$

3.20

And the transport equation for ε is modified through the multiplication of the production term by the coefficient C$_1$ described by:

$$C_1 = \max\left(0.43, \frac{\eta}{\eta + 5}\right)$$

3.21

Where

$$\eta = S\frac{k}{\varepsilon}$$

3.22

It has been observed that the realizable k-ε performs better than or equivalently to the standard k-ε model and shows improvement in prediction of shear flows. For these reasons the realizable k-ε has been chosen as a second baseline model for the work in this thesis.

3.2.4 Non-Linear Eddy Viscosity Models

One of the prime limitations in traditional eddy viscosity models is the linear relation between the Reynolds stress tensor and the stresses and strains in the resolved velocity field. This linear relation incorrectly describes the momentum transfer between residual and resolved fields. Non-linear eddy viscosity models (NLEVM) seek to overcome this limitation by introducing higher order relations for the Reynolds stress tensor.

In this work the Cubic NLEVM model of Baglietto and Ninokata (2006) was used for its robustness and accuracy under a wide variety of flow cases. The model was based on the NLEVM formulation of Shih et al. (1995); with the coefficients determined through DNS analysis on a variety of test cases. The formulation for τ_{ij} is:

$$
\begin{aligned}
\tau_{ij} = {}& \frac{2}{3} k \delta_{ij} - 2\mu_t \bar{S}_{ij} + 4C_1 \mu_t \frac{k}{\varepsilon} \left[\bar{S}_{ik}\bar{S}_{kj} - \frac{1}{3}\delta_{ij}\bar{S}_{kl}\bar{S}_{kl} \right] + 4C_2 \mu_t \frac{k}{\varepsilon} \left[\bar{\Omega}_{ik}\bar{S}_{kj} + \bar{\Omega}_{jk}\bar{S}_{ki} \right] \\
&+ 4C_3 \mu_t \frac{k}{\varepsilon} \left[\bar{\Omega}_{ik}\bar{\Omega}_{jk} - \frac{1}{3}\delta_{ij}\bar{\Omega}_{kl}\bar{\Omega}_{kl} \right] + 8C_4 \mu_t \frac{k^2}{\varepsilon^2} \left[\bar{S}_{ki}\bar{\Omega}_{lj} + \bar{S}_{kj}\bar{\Omega}_{li} \right] \bar{S}_{kl} \\
&+ 8C_5 \mu_t \frac{k^2}{\varepsilon^2} [\bar{S}_{kl}\bar{S}_{kl} + \bar{\Omega}_{kl}\bar{\Omega}_{kl}]\bar{S}_{ij}
\end{aligned}
$$

$$3.23$$

Where the non-constant coefficients are:

$$
C_\mu = \frac{C_{a0}}{C_{a1} + C_{a2}\bar{S}^* + C_{a3}\bar{\Omega}^*} \qquad C_1 = \frac{C_{NL1}}{(C_{NL6} + C_{NL7}\bar{S}^{*3})C_\mu}
$$

$$
C_2 = \frac{C_{NL2}}{(C_{NL6} + C_{NL7}\bar{S}^{*3})C_\mu} \qquad C_3 = \frac{C_{NL3}}{(C_{NL6} + C_{NL7}\bar{S}^{*3})C_\mu}
$$

$$3.24$$

$$
C_4 = C_{NL4}C_\mu^2 \qquad C_5 = C_{NL5}C_\mu^2
$$

The constants used are shown in Table 3.2.1.

C_{a0}	C_{a1}	C_{a2}	C_{a3}	C_{NL1}	C_{NL2}	C_{NL3}	C_{NL4}	C_{NL5}	C_{NL6}	C_{NL7}
0.667	3.9	1.0	0.0	0.8	11.0	4.5	-5.0	-4.5	1000.0	1.0

Table 3.2.1 Cubic NLEVM constants of Baglietto and Ninokata (2006)

The transport equations for k and ε are those of the standard k-ε of Launder and Spalding (1974).

The Cubic NLEVM of Baglietto and Ninokata (Baglietto and Ninokata, 2006) was used as the foundation for the Hybrid turbulence model STRUCT (Lenci, 2016) used in this work and as such the NLEVM was tested both as a baseline turbulence model and in the STRUCT model. The STRUCT hybrid turbulence model will be discussed further in 3.2.7.

3.2.5 Large Eddy Simulation

Large Eddy Simulation (LES) methods utilize a fundamentally different conceptual modeling technique from RANS to obtain simplified equations which may be solved on grids coarser than required for DNS. In LES a filter is applied to the Navier-Stokes equations separating it into the sum of the resolved (filtered) and residual (modeled) fields. The filter is related to the length and time scale at which eddies are assumed to take a universally isotropic behavior which is typically linked to the grid size used. Therefore, the eddies larger than the grid size are directly resolved (as the filtered equations) and the effect of the eddies smaller than the grid on the larger eddies is modeled through a sub-grid-scale (SGS) model. The SGS model is typically simpler than RANS eddy viscosity models by relying on the simplicity afforded by the isotropic eddy assumption at small scales. However, the grid size must be sufficiently fine for such an assumption to hold true – and as such LES is significantly more computationally intensive than RANS based methods. Proper application of LES typically requires the resolution of at least 80% of the energy everywhere in the domain (Pope, 2001).

Although many different SGS models exist, their effect on well behaved non-reacting flows –especially far from the wall – is often much smaller than the effect of different RANS models. This observation, in addition to the extreme cost of performing an LES simulation, motivated the study of only the wall adapting local eddy viscosity (WALE) LES model of Nicoud and Ducros (1999) in this work.

The WALE closure relates the residual stress tensor to the resolved tensor through an eddy viscosity, where the eddy viscosity is solved as:

$$\mu_t = (C_w \Delta)^2 \frac{\left(\bar{S}_{ij}^d \bar{S}_{ij}^d\right)^{3/2}}{\left(\bar{S}_{ij} \bar{S}_{ij}\right)^{5/2} + \left(S_{ij}^d S_{ij}^d\right)^{5/4}} \qquad 3.25$$

Where $C_w = 0.544$, Δ denotes the grid size, and $\bar{S}_{ij}^d$ is as:

$$\bar{S}_{ij}^d = \bar{S}_{ik}\bar{S}_{kj} + \bar{\Omega}_{ik}\bar{\Omega}_{kj} + \frac{2}{3}\delta_{ij}(\overline{II}) \qquad 3.26$$

$\overline{II}$ is the second invariant of the resolved velocity gradient tensor, which physically represents the balance between resolved strain and shear rate. Such a term has often been linked to the eduction of turbulent coherent structures – which will be described further in this thesis. $\overline{II}$ is defined as:

$$\bar{II} = \frac{1}{2}(\bar{\Omega}_{mn}\bar{\Omega}_{mn} - \bar{S}_{mn}\bar{S}_{mn}) \qquad\qquad 3.27$$

This approach automatically takes into account the shear stress near the wall and has been shown to automatically obtain near wall scaling of the eddy viscosity.

3.2.6   Hybrid Turbulence Modeling

Hybrid turbulence models are a class of models that attempt to balance the accuracy of LES with the low cost and robustness of RANS models. This balance is predicated on the observation that although LES and RANS models have intrinsically separate theoretical foundations, they result in identical equations reliant on the eddy viscosity assumption. A very simple hybrid model could consist of simply averaging the eddy viscosity between RANS and LES models.

Three popular hybrid models will be briefly described to highlight the key features and inspirations for the STRUCT turbulence model. One of the earliest hybrid models, detached eddy simulation (DES) introduced by Spalart (1997) switches between URANS and LES predictions of eddy viscosity locally based on characteristic length scales. For airplane wing applications, for which it was first developed, this equates to solving a URANS model near the wall and LES in the far flow field. DES drastically reduces computational cost by avoiding the fine grid requirement near the wall for LES, but has shown general lack of robustness related to the grid size used and sometimes inappropriate switching locations for URANS and LES.

The scale adaptive simulation (SAS) model (Menter et al., 2003) uses a baseline URANS model with hybrid activation dependent on the length scales, strain rates, and other flow variables such as k and ω (when utilizing the k-ω SST as baseline). SAS achieves similar performance to DES while reducing grid sensitivity, however SAS does not always provide accurate physical descriptions.

The partially averaged Navier-Stokes (PANS) model of Girimaji et al. (2003) also uses a URANS baseline model that controls the resolution of turbulence through ratios between modeled and resolved turbulent kinetic energy as well as between modeled and resolved turbulent dissipation rate. The model is able to directly switch between URANS and DES based on these control parameters. The lack of a proper determination for the control parameters leads to a lack of generality for the PANS model.

3.2.7   STRUCT Turbulence Model

The work in this thesis implements heavily the controlled version of the STRUCT turbulence model. A brief introduction to the STRUCT model is provided here; a more thorough theoretical and numerical description of the model can be found in (Lenci, 2016).

As previously discussed the URANS decomposition separates the instantaneous flow field into a slowly varying time mean, and instantaneous fluctuating component. However, it is observed in many flow conditions that large scale turbulent "coherent" structures can form in a flow field. In these flow structures, the time scale of the resolved turbulence is higher than typical, and as such can overlap

29

with that of the modeled turbulence timescale. Such an overlap invalidates the basic assumption of the URANS decomposition – that there is a separation of scales between the modeled and resolved turbulence. The high frequency of the coherent structure is mistakenly "seen" by the URANS models as the same as random turbulent fluctuations, and as such the eddy viscosity is "over-predicted" by the model. The eddy viscosity destroys the detailed information about the structure itself, which in reality should persist for a time and length scale larger than that of incoherent turbulence. Such a destruction of information about the structures in the flow can render even mean quantity predictions completely inaccurate.

The STRUCT model builds upon this observation by reducing the assigned eddy viscosity inside the coherent structures. This approach requires two independent parameters: an eddy viscosity reduction factor and a coherent structure eduction method, neither of which are trivial to ascertain. The approach can be summarized as in (Lenci, 2016) as:

$$\frac{k_m}{k_{tot}} = \begin{cases} 1 \\ \phi \end{cases} \quad if \quad \begin{array}{c} h \leq 1 \\ h > 1 \end{array} \qquad 3.28$$

Where

$$h = \frac{f_r}{f_{URANS}} \qquad 3.29$$

and

$$f_r = \sqrt{|\overline{II}|} \qquad 3.30$$

$$f_{URANS} = \frac{\varepsilon}{k} \qquad 3.31$$

The terms in Equations 3.30 and 3.31 represent the frequency of the resolved and modeled scales respectively. The model is activated in regions of sufficiently high $\overline{II}$ i.e. coherent structures. A slightly altered formulation from Acton el al. (2015) is used in this work as:

$$\mu_t = \begin{cases} \mu_t \\ \phi\mu_t \end{cases} \quad if \quad \begin{array}{c} f_r < f_{r,0} \\ f_r \geq f_{r,0} \end{array} \qquad 3.32$$

Where

$$f_r = \sqrt{|\overline{II}|} \qquad 3.33$$

As can be seen STRUCT borrows from PANS and SAS models, activating based on time scales and controlling resolution by a factor controlling the ratio of modeled to total turbulent kinetic energy as in (Lenci, 2016) or directly the eddy viscosity as in (Acton et al., 2015).

The work shown here determined the optimal settings for ϕ and $f_{r,0}$ for each flow case tested through testing and visual inspection of the flow. The exact parameters utilized will be discussed in the following sections.

Lenci (2016) has recently introduced two complete formulations requiring no a priori specification of parameters, such an approach is only lightly discussed in this work.

4 JAEA Triple Jet Test Case

The JAEA triple jet test case, described in section 2, was chosen as one of three test cases for this work due to its relative geometric simplicity, representativeness of thermal striping, and widespread study in the literature by numerous authors.

4.1 Description

The triple-jet experiment performed by Tokuhiro and Kimura (1999), shown in Figure 2.2.1 and Figure 4.1.1, utilized a large tank for the mixing of three jets of fluid at two different temperatures. Blocks were used to create rectangular inlet flows. The jets were bounded on two sides by separation plates extending far enough to isolate the flow in the mixing area of study. The experiment was conducted at a range of temperatures, delta temperatures, and velocities.

In this study, only the case where the temperature of the jets was 25 °C and 30 °C, and velocities of all jets are 0.5 m/s is considered. The Reynolds number at the outlet of the center nozzle, calculated using the hydraulic diameter of the inlet jet, is 1.8E4. Velocity profiles were measured with an Ultrasound Doppler Velocimetry (UDV) system, while temperature profiles were measured with a traversing tree of 39 thermocouples.
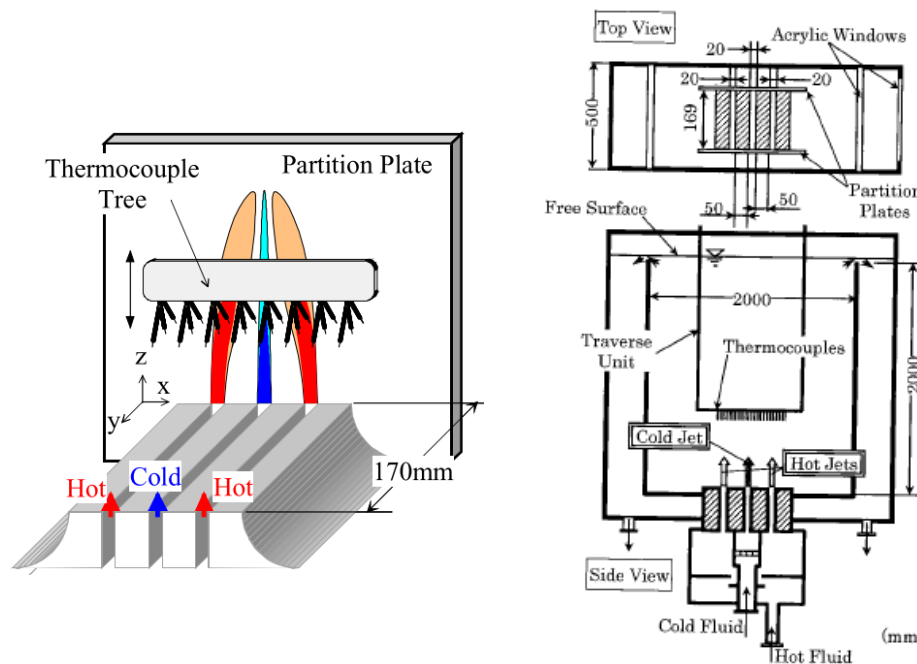

Figure 4.1.1 Experimental configuration of the JAEA triple jet experiment. Taken from (Kimura et al., 2002)

As previously discussed in section 2, Nishimura and Kimura (2003) and others have shown the limitations of traditional URANS models for prediction of mean and fluctuating profiles of temperature and velocity – as well as prediction of dominant fluctuation frequencies.

However, Jung and Yoo (2004) and Cao et al. (2012a) have shown the successful application of an LES model, and in addition, Kimura et al. (2002) showed improved predictions by using no turbulence closure. For these reasons the standard linear k-ε, the cubic k-ε of Baglietto and Ninokata (Baglietto and Ninokata, 2006), the WALE LES, and the no closure models will be tested against that of the STRUCT hybrid turbulence model introduced in section 3.

4.2   Simulation Setup

All analyses are performed using the commercially available finite-volume CFD code STAR-CCM+ version 9.04.011, while a development version is adopted for implementation of the STRUCT model. A segregated flow solver based on the SIMPLE algorithm applied on co-located variables with Rhie-Chow interpolation is leveraged. The segregated fluid energy formulation is used, which solves an additional transport equation as part of the SIMPLE iterations, according to which temperature is determined (CD-adapco, 2014). The Boussinesq approximation is adopted to account for the effects of buoyancy, following the approach of Durve et. al (2010), and owing to the small density variation for water between 25 °C and 30 °C (< 0.1%).

All convective terms are approximated with an upwind-based non-oscillatory 2nd order scheme, using the Venkatakrishnan reconstruction gradient limiting. For LES simulations, a locally-bounded central-differencing (BCD) scheme is adopted for the convective terms. The Hybrid Gauss LSQ gradient reconstruction method with 2nd order time integration is used. The time step in each case is determined by the requirement of Courant number lower than 1. The simulation is run for a total of 125 seconds, with the start of statistics sampling occurring at 20 seconds – the time at which stable oscillations are present. The statistics were sampled for 105 seconds, which was determined to be conservatively sufficient for complete convergence of all physical parameters.

The computational domain is simplified to include only the regions of interest in the experimental setup and is shown in Figure 4.2.1 following the common computational simplifications performed in the literature. The size of the simulated region is 300(x) x 60(y) x 600(z) mm plus three identically sized inlet channels measuring 20(x) x 60(y) x 600(z) mm. The inlet channels are extruded to 600 mm to create fully developed profiles in the simulation. A fine 1 mm computational grid was created as optimal mesh for LES simulations, while a coarser 4 mm grid was created on which to compare all the turbulence models. Tests on even coarser grids, not shown here, confirmed that good grid convergence is achieved for the URANS and STRUCT models in the 4 mm grid. The wall function utilized requires a non-dimensional y+ value over 30. This requirement is satisfied with a 4 mm cell at the wall.
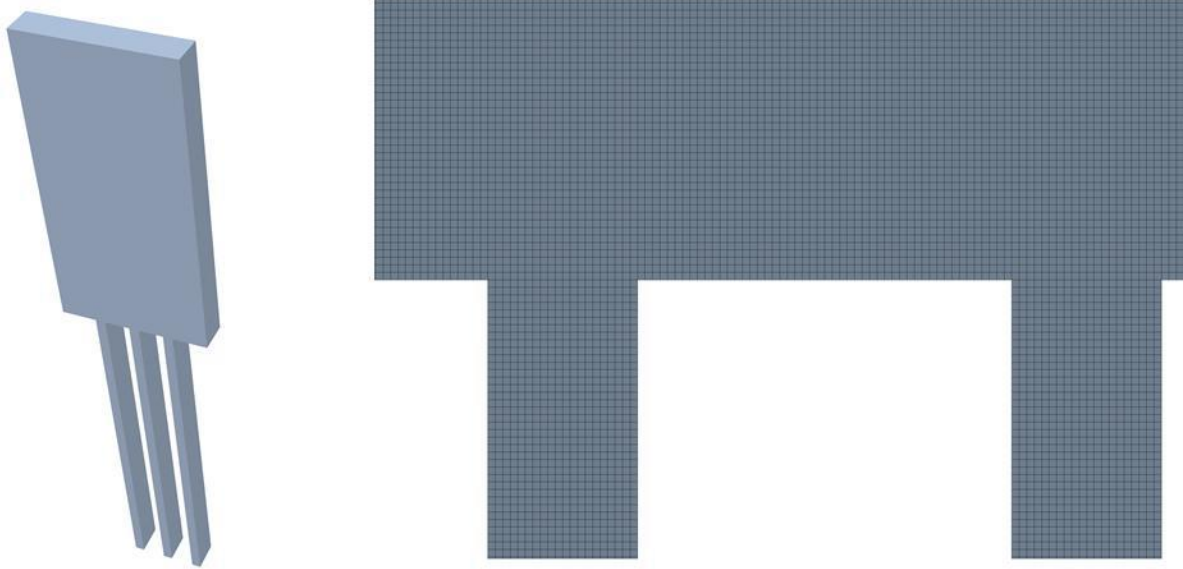
Figure 4.2.1 Computational domain, and detail of the 1 mm isotropic hexahedral trimmed mesh.
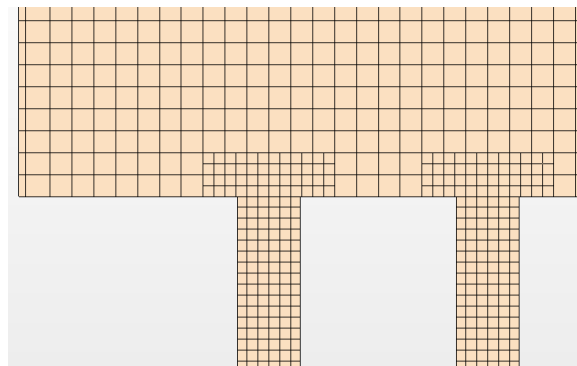
Figure 4.2.2 Detail of the 4mm / 2mm isotropic hexahedral trimmed mesh.

4.2.1   *Boundary Conditions*

A flat velocity profile of 0.5 m/s is used at the inlet of the extruded channels as boundary condition. The inlet temperature is specified as 25 °C in the central channel and 30 °C at the two sides. The walls in the experiment are set as no-slip boundary conditions, while the two lateral and ceiling boundaries are set as the pressure outlet boundary condition available in STAR-CCM+ (CD-adapco, 2014). The pressure outlet condition extrapolates the boundary face velocity from the interior cells, allowing outflow and inflow. The entire region as well as the pressure outlets are initialized to the mean mass flow mixing temperature of 28.33 °C, and the same temperature is used for reverse flow at the pressure outlets. Other parameters used for such reverse flow are a turbulence intensity of 0.25 and a turbulent viscosity ratio of 90, as determined during separate test simulations.

A sensitivity study was performed to determine the impact of the chosen simulation domain and boundary conditions. The two main parameters of interest were the boundary specification of the side regions, and their location in the domain. These parameters are of key interest because they are

the most significant simplifications of the physical domain, which is depicted in Figure 4.1.1. In addition, the effect of the inlet nozzle shape – shown in Figure 4.2.3 - and thermocouples on the flow structure was not considered.
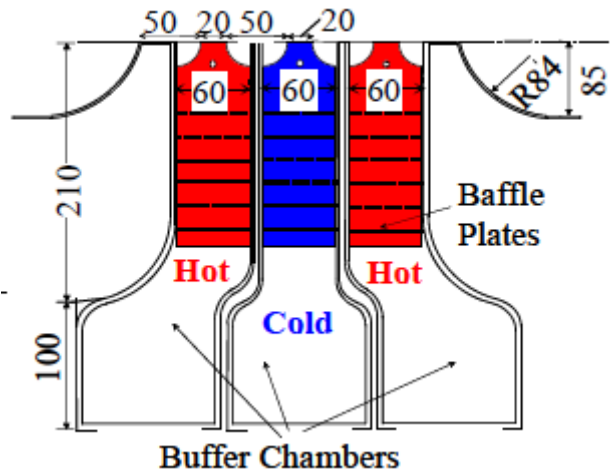
Figure 4.2.3 JAEA triple jet experiment inlet nozzle configuration. Taken from (Kimura et al., 2007b)

It was determined through extrusion of the side boundaries by 70 mm increments up to a total of 350 mm that the standard geometrical set point for the side walls was sufficiently far from the location of important flow evolution as to not have any significant effect.

The impact of the specification type of the side boundaries was found to have a dominant effect on the flow. Both slip and no-slip wall boundaries introduced instability in the flow that caused flow "sticking" to the wall for all turbulence models and all extrusion lengths tested. This effect is depicted clearly in Figure 4.2.4. This behavior, known as the Coanda effect (Wille and Fernholz, 1965), is physically possible for conditions in which wall boundaries are appropriate, but is unphysical for simulations where this wall boundary is actually an open boundary.

Figure 4.2.4 LES of original domain – fine mesh (left) and linear k-ε of 2X extruded domain – coarse mesh (right) showing non-physical flow "sticking".

This effect is also noticed in the work by Omotowa et al. (2012) on a twin jet investigation with OpenFoam and COMSOL using wall boundaries. Based on the experimental data by Tokuhiro and Kamide (1999) and the sensitivity study performed here, an equivalent to the STAR-CCM+ pressure outlet boundary condition is recommended for similar flow investigations.
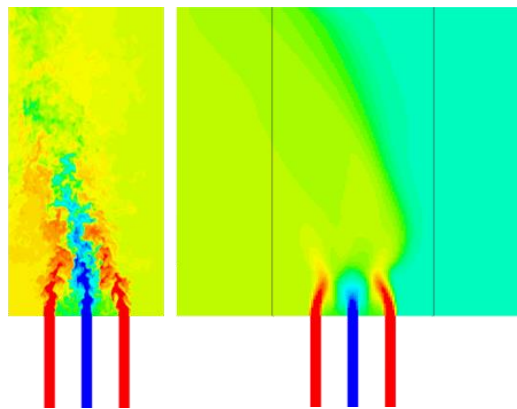
4.3 Results and Discussion

The turbulence closure approaches illustrated in Section 2 plus an unclosed formulation (solution of Navier Stokes without any subgrid stress), as discussed in Section 3.1, are tested on the coarser grid, while LES is performed on the appropriately finer grid for comparison. Parameters used for the STRUCT approach are ϕ = 1E-5 and f_r = 1.4; these optimal values were determined through testing and a posteriori averaging of the flow structures. Results using the STRUCT approach show higher accuracy over all forms of URANS tested, and improvement over LES. Results are presented on the same figures to better appreciate trends, also in comparison to experimental data. All simulation results reported are taken at the mid-plane location, between the two isolation plates. Figure 4.3.1 depicts the instantaneous temperature profiles along with an image of the flow extracted from the experiment.
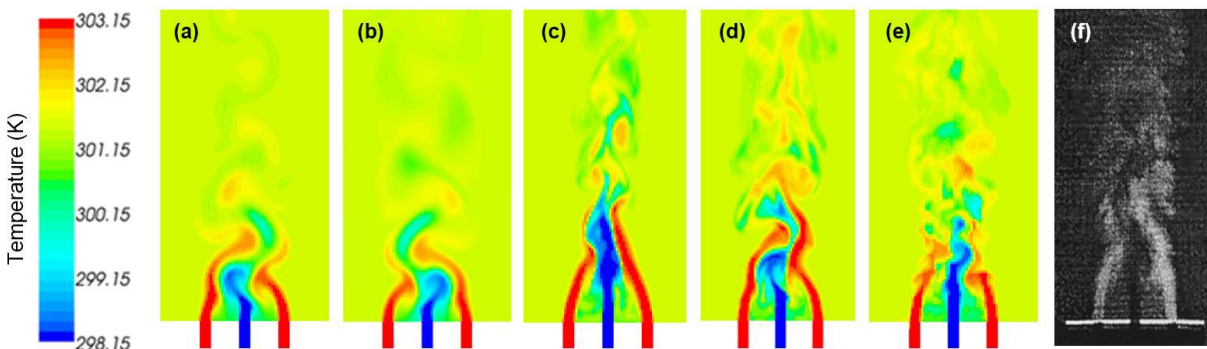
Figure 4.3.1 Instantaneous temperature distribution: (a) Realizable k-ε, (b) cubic k-ε (c) no-closure (d) STRUCT (e) LES (f) Experiment figure (f) taken from (Tokuhiro and Kimura, 1999)

As a massively separated flow it can be predicted that the presence of highly energetic large scale coherent structures will be critical to the flow description. Such a test case is similar to the classic test case of flow past a square cylinder, showing the formation of Von Karman vortices. This prediction is confirmed by Figure 4.3.2, showing the formation of large scale coherent structures in the domain. The performance of the STRUCT model is tied closely to these turbulent structures, the activation regions of the model are shown in Figure 4.3.2.
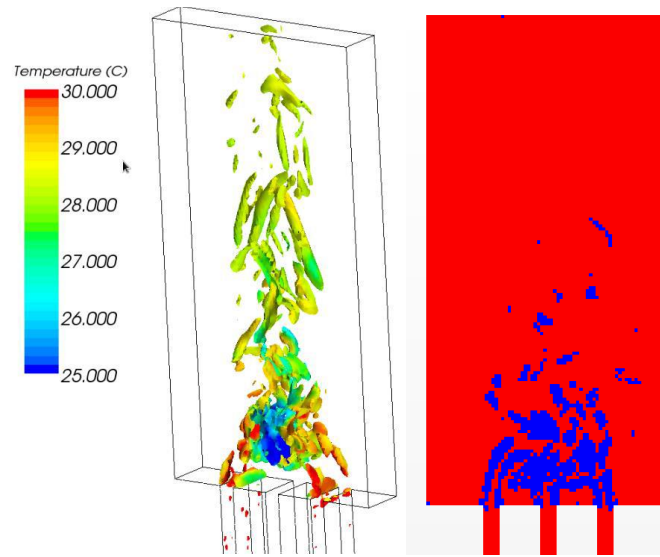
Figure 4.3.2 Iso-surface of the absolute value of q-criterion, colored by temperature (left) showing regions of coherent structures, and STRUCT model activation in blue (right)

In the following figures only the 4 mm results are plotted for the LES simulations, since the results are very close to those of the 1 mm simulation.

Time-averaged velocity profiles have been plotted in Figure 4.3.3. All models are able to successfully predict the velocity profiles at all data levels except for the 2nd and 3rd level, which correspond to the heights at which most mixing is experimentally observed. At these heights, a behavior of both URANS models, i.e. the realizable k-ε and the cubic k-ε, to over predict mixing is observed, showing a flattening of the velocity profile much earlier than what is measured. This over prediction of mixing is due to the over prediction of eddy viscosity in the turbulent coherent structures as discussed in section 3; such a behavior artificially increases the effective viscosity of the fluid. The increased viscosity is responsible for a reduction of momentum transfer along the length of the domain. The LES, STRUCT, and no closure methods can successfully capture the behavior on the 2nd data level, while over predicting the velocity gradients on the third level. At this height, only the STRUCT method captures the velocity above the center jet, while slightly over predicting the one above the outer jets.
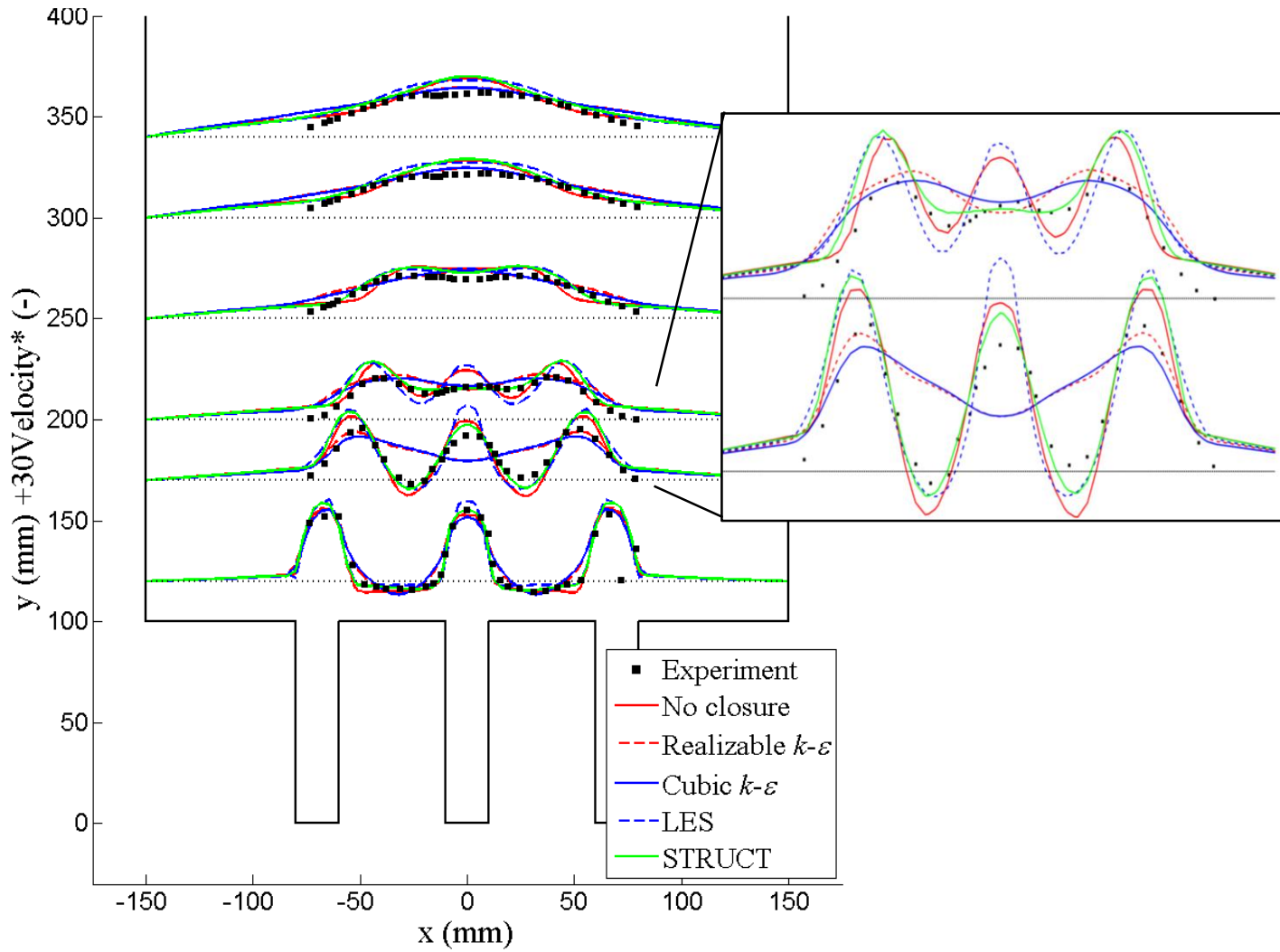
Figure 4.3.3 Time averaged velocity profiles for the 4 mm mesh.

Figure 4.3.4 shows the time-averaged temperature profiles for the different models tested. However, as it will be shown later in Figure 4.3.5, only the finer-mesh LES provides a good description of the temperature fluctuation frequency. This parameter is very important in thermal striping analysis, and indicates that the good profile prediction from the coarser LES is likely an artifact of the averaging process, rather than a reliable LES capability.
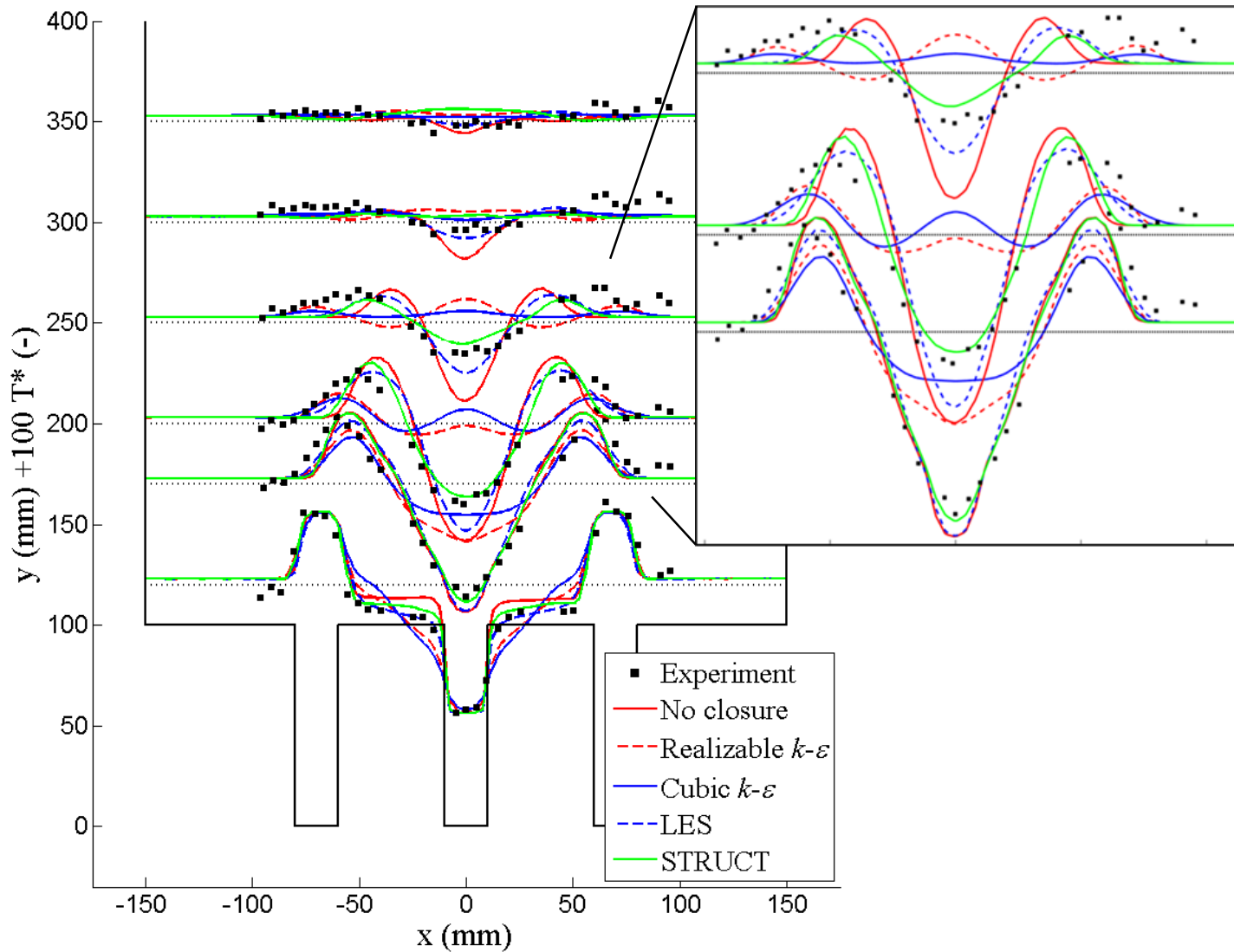
Figure 4.3.4 Time averaged temperature profiles for the 4 mm mesh.

The LES and the STRUCT method match the experimental data much closer than other approaches, which introduce a significant error either in the lower (URANS) or middle (no closure) part. These inaccuracies are due to the inadequate description of the mixing phenomena, also evident in the velocity profiles.

The normalized temperature fluctuation intensity is of significant importance to thermal striping analysis because it is the mechanism by which temperatures are absorbed by the surrounding materials. Profiles are plotted in **Error! Reference source not found.**. The dimensionless temperature used is defined as in (27), where T_h, T_c and T_{avg} are respectively the temperature of the hot inlets, the cold inlet, and the mass-flow-rate-weighted average.

$$T^* = \frac{T - T_{avg}}{T_h - T_c} \qquad\qquad 4.1$$
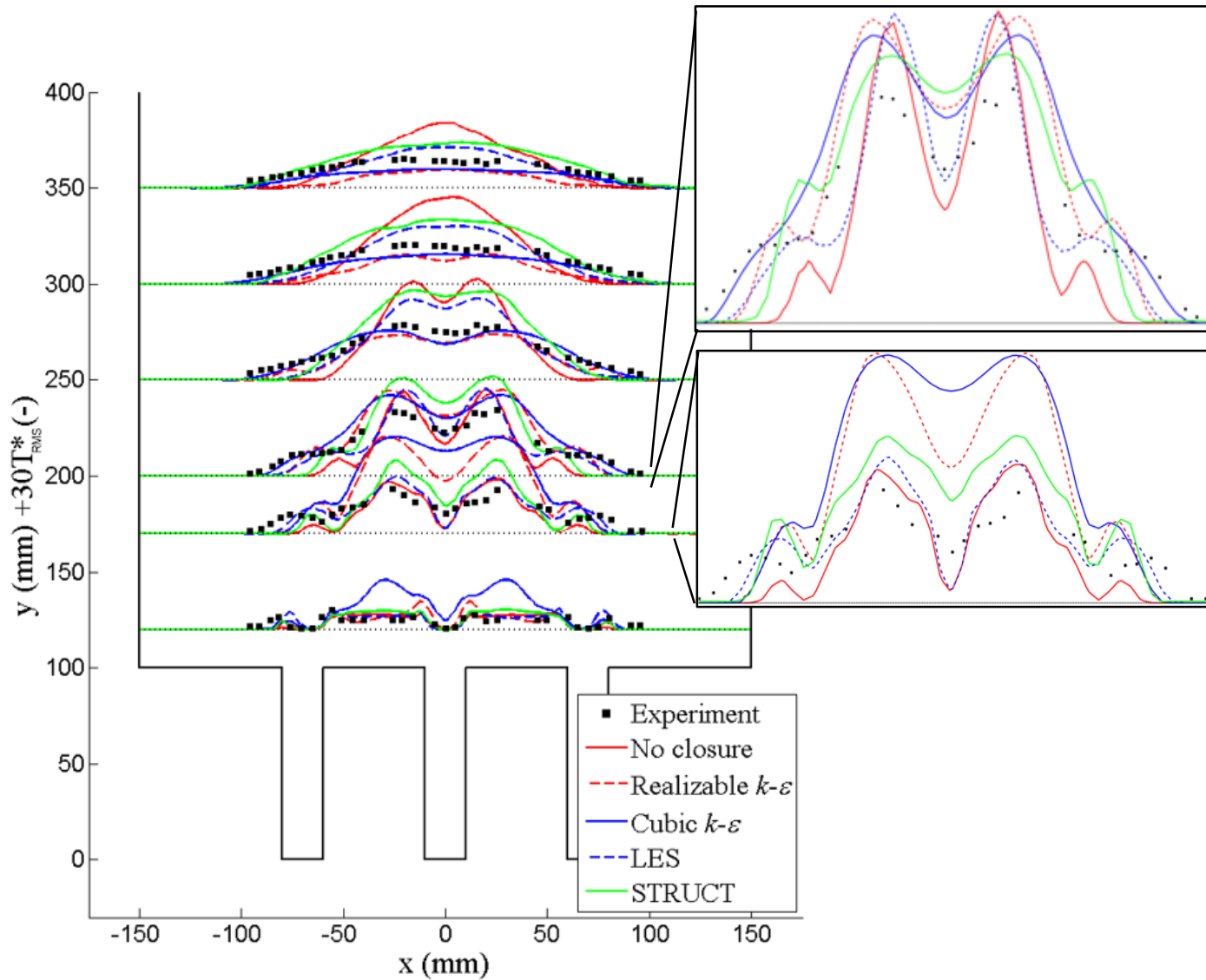
Figure 4.3.5 RMS Temperature profiles for the 4 mm mesh.

The realizable k-ε and the cubic k-ε models strongly over predict the temperature fluctuations at the lowest levels. Again, this is related to an over prediction of mixing at the lowest elevations, evident in Figure 4.3.3, and Figure 4.3.4. The LES, STRUCT, and no closure methods all capture the fluctuations well at the lower levels, while slightly over predicting fluctuations at the higher ones – indicating an over prediction of spatial coherence of the turbulent structures as compared to experimental measurements. An over prediction of fluctuations at the center is shown in the result with no closure at the upper level.

As a quantitative evaluation of each model's performance in matching experimental values, the figure of merit (FOM) in the following equation is adopted.

$$FOM = \sum (X_{exp} - X_{model})^2 \qquad\qquad 4.2$$

This quantity represents the sum of the variance between the experimental measurement and the model prediction over all experimental points. This value is further normalized by the FOM for the realizable k-ε in each case. A value below unity indicates superior performance compared to the realizable k-ε model. This FOM was chosen to place equal weight in all experimental data positions, but to place added emphasis on severe failures of model predictions. The FOM for each model in predicting the values of velocity, temperature, and temperature fluctuation intensity are shown in **Table 4.3.1**.

	Mean Velocity	Mean Temperature	RMS Temperature	Average FOM
No Closure	0.91	0.56	1.52	0.99
Realizable k-ε	1.00	1.00	1.00	1.00
Cubic k-ε	0.98	1.35	1.41	1.25
LES	1.20	0.31	0.55	0.69
STRUCT	0.98	0.31	1.17	0.82

Table 4.3.1 FOM for each model and variable of interest.

Finally, the dominant frequencies of temperature fluctuation are of critical importance for determining the attenuation of temperature variation in materials. The normalized power spectral densities of the different models at the experimental measuring point, x = -15 mm, y = 0 (centerline), z = 100 mm, are shown in Figure 4.3.5. The experiment yields a dominant frequency of approximately 2.3 Hz. This value is best predicted by the cubic k-ε (~2.28 Hz) and the STRUCT approach (~2.38 Hz). The realizable k-ε and the no-closure method both provide a significantly inaccurate dominant frequency. The fine-mesh LES predicts the fluctuation frequency within 5% to about 2.45 Hz. However, lack of accuracy of the coarser mesh LES is evidenced by many dominant frequencies, all of which poorly match the observed frequency.

In conclusion, on the 4 mm mesh, results obtained with the STRUCT approach are the ones that most closely match the experimental description of thermal striping.
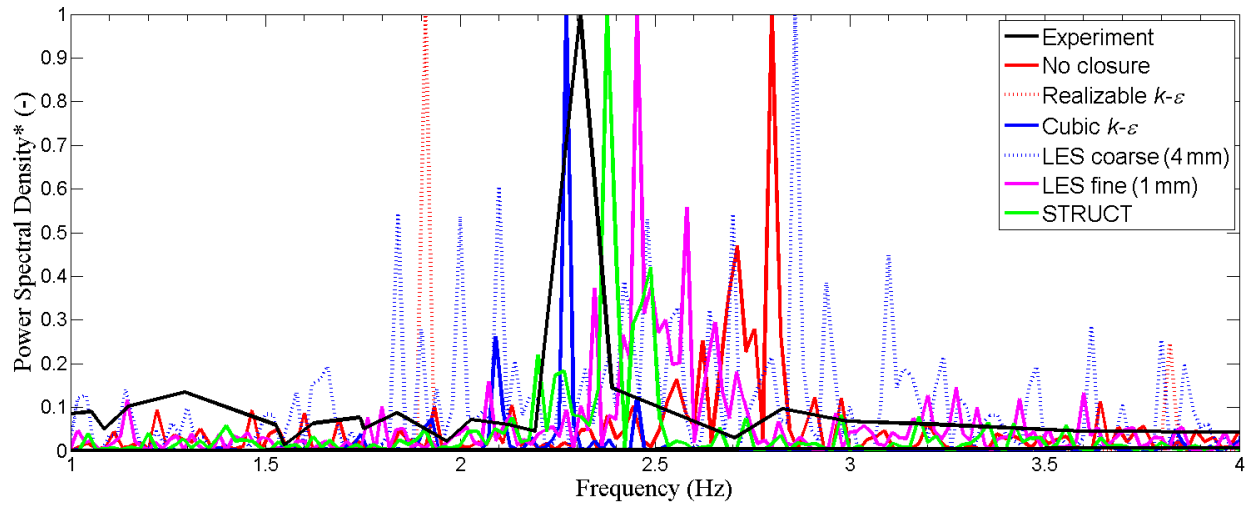
Figure 4.3.5 Normalized power spectral densities of temperature fluctuation. All models are applied to the coarser (4 mm) mesh, except for LES, which is applied to both meshes, as defined in the legend.

5   PWR Assembly Test Case

In pressured water reactors (PWR), mixing vanes are installed in the coolant sub-channels to increase the average heat transfer coefficient in the channels and to improve the departure from nucleate boiling (DNB) performance. These mixing vanes are also responsible for fluctuating forces on the fuel rods, which can cause vibration induced fatigue and failure in a process known as grid-to-rod-fretting (GTRF). This phenomenon was chosen as a relevant test case for thermal striping flows because it represents a flow configuration that is highly challenging for current turbulence modeling approaches. It is shown here that the presence of large scale swirling coherent structures causes fluctuating forces on the fuel rods. Such a test case, exhibiting an extremely complex and turbulent flow configuration with large scale coherent structures is relevant for SFR internal flows as it has shown a clear-cut character, where all URANS approaches drastically fail and only accurate LES methods have shown reliable predictions. While no direct measurement exists for the configuration discussed in this work, evidence is provided to justify the confidence in the predictions.

This section will first discuss the previous work in this area, then the simulation setup and computational details, and finally will discuss the results of this study. The focus of this task is to predict the fluctuating forces on the fuel rods accurately, which can then be used to couple with structural analysis codes to predict GTRF.

5.1   Previous Work

Fuel rod vibrations can be classified on the basis of the driving mechanisms, which can be either internal or external to the fuel assembly of interest (Kim, 2009). As discussed by Kim and Suh (2009) these vibrations are related to various engineering parameters such as inter-fuel assembly gaps, water to fuel ratio, inlet nozzle design, etc. However, Kim (2010) indicated that the design of the spacer grid mixing vanes is the dominant cause of fuel rod vibrations. The mixing vanes introduce non-axial flow direction to increase the heat transfer coefficient of the coolant while also strongly increasing the level of turbulence.

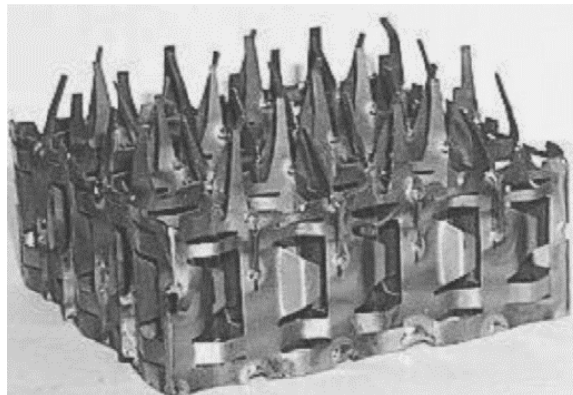An example PWR spacer grid with mixing vanes is shown in Figure 5.1.1.

Figure 5.1.1. Example spacer grid with mixing vanes. Taken from (Lee and Choi, 2007)

Delafontaine and Ricciardi (2012) theorized that the root cause of the fluctuating forces is due to quasi periodic coherent structures occuring between tightly spaced rod bundles. As mentioned by Delafontaine and Ricciardi (2012), these coherent structures have been observed in the same frequency range by Chang and Tavoularis (2008) and Baratto et al. (2006). However, this work demonstrates that the fluctuating forces are caused by mixing vane generated coherent structures, rather than the quasi-periodic structures generated between rod bundles.

CFD simulations of PWR assembly flow using the RNG k-ε (Conner et al., 2010) and realizable k-ε (Yan et al., 2011) turbulence models have been validated successfully against experimental data for mean velocity profiles. However, those RANS based methods do not provide reliable information on fluctuating flow fields as needed to predict GTRF. As a consequence, Okui et al (2013) utilized an empirical correlation to approximate the fluctuating forces only from information on the mean flow velocity. However, such an approach relying upon empirical correlations is not desirable from a design perspective, and as such most studies have focused on the use of LES turbulence modeling to calculate the turbulent forces. LES results have been widely validated against experiments in single-rod simulations by Ikeno and Kajishima (2006), Bieder et al (2015), and Delafontaine and Ricciardi (2012), and in 5x5 rod bundles by Bakosi et al (2013).

Elmahdi et al (2011) coupled the LES predictions of the fluctuating forces with the Westinghouse vibration analysis code VITRAN. The fuel rod vibration amplitude was accurately predicted by VITRAN in comparison to experimental data. The VITRAN code itself has been separately validated with experimental data from the VIPER flow loop (Lu et al., 2011). Moreover, Liu et al (2013) directly coupled the fluctuating forces to a structural code, and Benhamadouche et al (2009) coupled the fluctuating forces to an analytical result obtained with Euler's beam theory. However, the latter two methods have not been validated against experimental data, and as such, the approach will follow the validated approach of Elmahdi et al (2011) in calculating the turbulent forces, which may be used in a dedicated vibration analysis code.

In this work different turbulence modeling approaches are utilized to predict the turbulent forces, comparing to the validated LES data presented by Elmahdi et al (2011). This work analyzes the impact of mixing vane generated coherent structures, showing that these structures cause the fluctuating forces on the fuel rods.

5.2   Simulation Setup and Computational Details

All simulations were performed with the commercial finite volume CFD code STAR-CCM+ version 10.02.010. The basic solver setup is consistent with previous applications, where the pressure-velocity coupling was performed with a segregated flow solver using the SIMPLE algorithm with 8 inner iterations. All URANS based methods utilized a 2nd order upwinding method with Venkatakrishnan gradient limiters for calculating the interpolation of convective fluxes; the LES method utilized a bounded central differencing technique. The segregrated fluid isothermal approach was used, with all parameters evaluated at 250 F. The Reynolds number of the flow is 1.2E5 based on the hydraulic diameter of the sub-channels.

All simulations were performed in unsteady mode, with a second order implicit temporal discretization, using a timesetp to ensure a courant number below 1. The simulation was performed for 2s, with statistics being collected at 0.4 seconds (representing 5 flow throughs), at which time the physical variables reached an unsteady convergence.

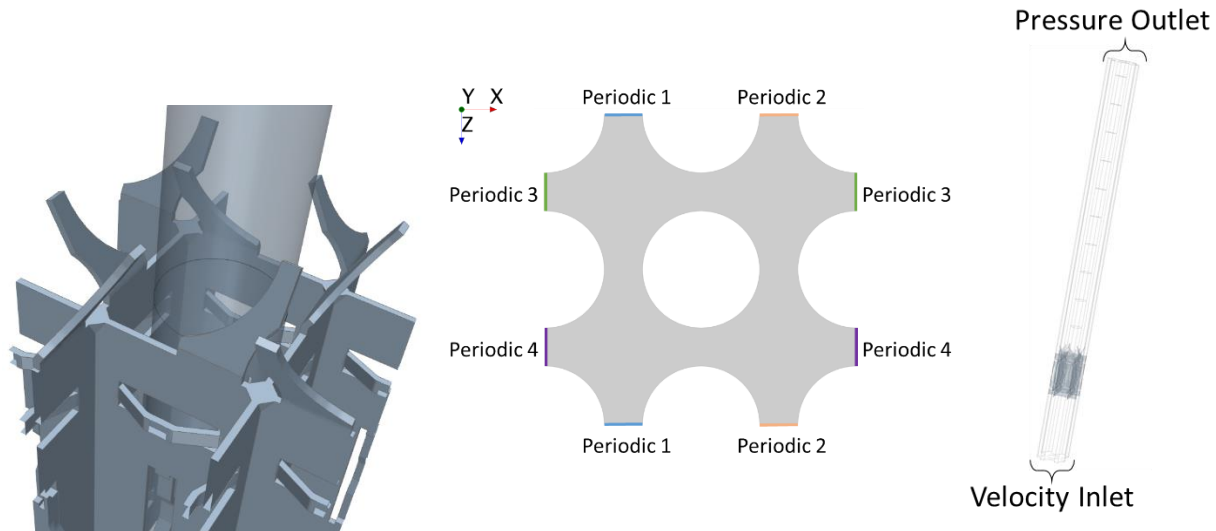The geometry and the computational domain are shown in

Figure 5.2.1 Spacer grid and rod configuration (left) and boundary conditions applied to the domain (center and right)

The domain consists of 4 subchannels from a standard Westinghouse 17x17 rod assembly corresponding to a rod pitch of 12.6 mm and a rod diameter of 9.6 mm. As mixing vanes and spacer grids are proprietary, here a surrogate design representing a standard mixing vane based on open literature is used.

All physical walls, such as the spacer gird, mixing vanes, and rod segments are modeled as no-slip boundary conditions. The spaces between the outer rod segments are modeled as periodic boundary conditions as shown in Figure 5.2.1. The inlet of the domain is set as velocity inlet, while the outlet is set as a pressure outlet boundary condition. The geometric set up and modeling follows that of Elmahdi et al (2011) in order to compare directly the prediction of excitation forces along the rod.

5.2.1 Meshing Strategy

Both a fine LES suitable mesh and a coarse URANS style mesh were used in this work. The fine LES mesh adopts the wall modeled LES approach, where standard wall fucntions are couple to the LES solution, as discussed in Elmahdi et al (2011) and reviewed accurately in Jayaraju et al (2010). The computational mesh used 0.14 mm size cells, with a 2 cell prism layer of 0.208 mm – resulting in a mesh of approximately 40 million cells. This prism layer was verified to produce a minimum y+ > 30 at all locations in the simulation domain. The coarse mesh used 0.4 mm size cells in the bulk domain and 0.2 mm size cells near the spacer grid along with a 1 cell prism layer of 0.35 mm. The departure

of meshing strategy for the coarse mesh from the fine mesh near the mixing vane is explained by the need for a maximum cell size of approximately 0.2 mm to adquately describe the geometry and ensure convergence. For both meshes, anisotropic cells of aspect ratio 1.35 were utilzed far from the spacer grid. The two meshes used in this study are shown in Figure 5.2.2.
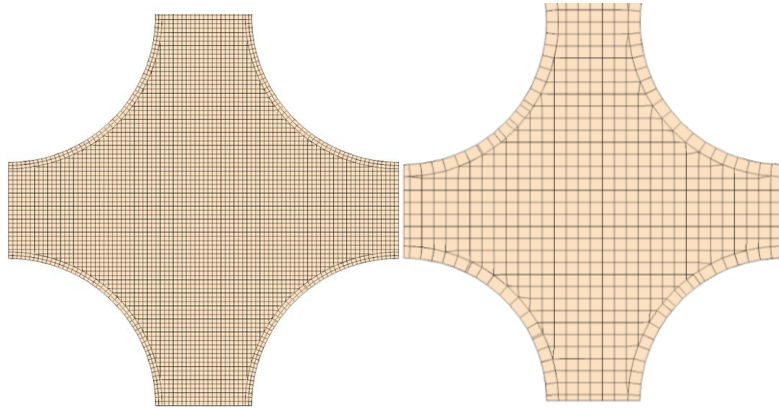

Figure 5.2.2 Close-up view in one sub-channel of the fine mesh (left) and coarse mesh (right)

5.3 Results

The goal of this study is to predict the RMS of the forces along the rod segments, and to compare these results to the VITRAN validated results shown in Figure 5.3.1. This is first done by validating the applicability of the surrogate spacer design through LES simulation and then prediction to Elmahdi et al (2011). After this validation, coarse mesh STRUCT results are compared to that of the LES simulation.
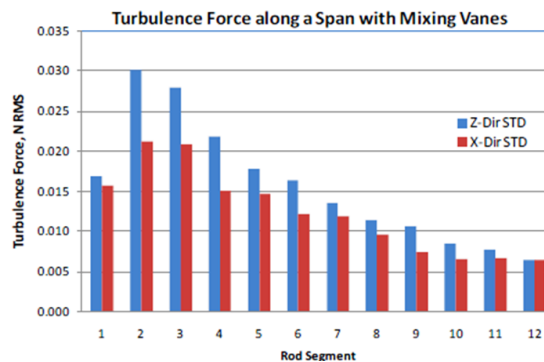
Figure 5.3.1 RMS forces on rod segments taken from (Elmahdi et al., 2011)

Five separate tests were performed for this work. In order to validate the computational model and simulation setup, the WALE LES model was utilized on the fine mesh, which as can be seen in Figure 5.3.2 match favorably with those of Elhamdi et al (2011). It is important to note that the study of Elmahdi et al (2011) used a proprietary spacer design so exact simultude is not expected. The main

difference between the LES results of the studies is the increased magnitude of the first three rod segments in the work performed here; the overall trends are matched for both studies.

The cubic k-ε model, which has been extensively validated for these applications (Baglietto and Ninokata, 2007, 2006; Brewster et al., 2015; Merzari et al., 2009) is tested on both the fine and coarse meshes. It can be seen the model fails to accurately predict the magnitude and trend of the RMS forces along the rod segments. Finally, the STRUCT turbulence model is tested on both the fine and coarse meshes as well. It can be seen that STRUCT on both meshes predicts the trend of RMS forces well, and that the magnitude of the prediction is reasonably accurate. The predicted RMS forces are shown in Figure 5.3.2.

Since it is of particular interest to this study, let us discuss the performance of the STRUCT turbulence model on the two meshes used. For this work, the LES model of Figure 5.3.2 is to be considered the baseline "correct" model, since exact agreement with the LES of Elmahdi et al. (2011) is not expected due to differences in spacer grid designs used.

It can be seen that the STRUCT model on the 40 Million cell mesh over predicts by up to 25% the RMS force along rod segments 1, 2, and 3. However, the STRUCT model on the coarse mesh under predicts the RMS force on rod segment 1 by over 30% while matching the predictions on rod segments 2 and 3 quite well. Part of the explanation for the slightly better performance of STRUCT on the coarse mesh is not related to improved description of the flow, rather the coarse mesh generates larger structures that compensate for the lack of resolution. Significant testing also indicates that in the adopted formulation of the model results depend sensibly on the selection of the ϕ and f_r parameters. This is not surprising, as the model adopted is not closed; on the other hand, the work of Lenci (2016) has recently proposed a fully closed version of the model that could be evaluated in future work.
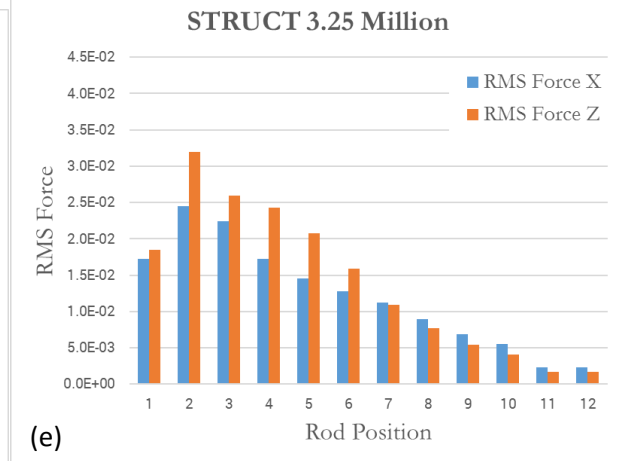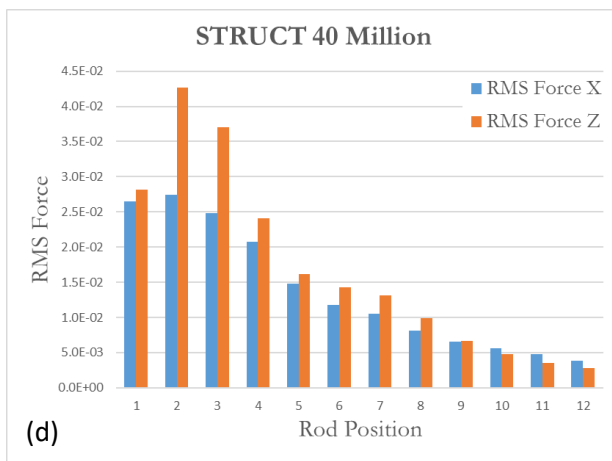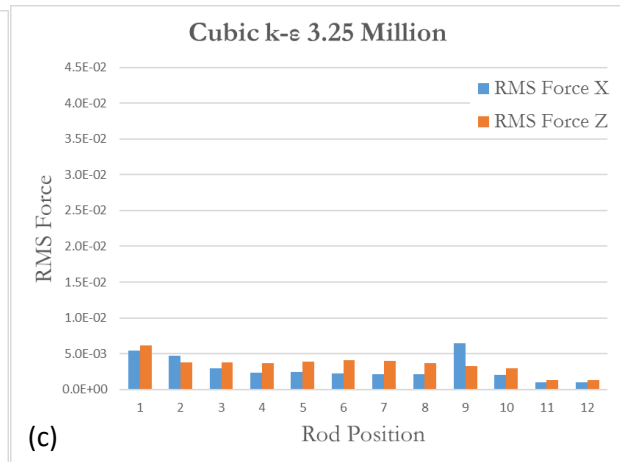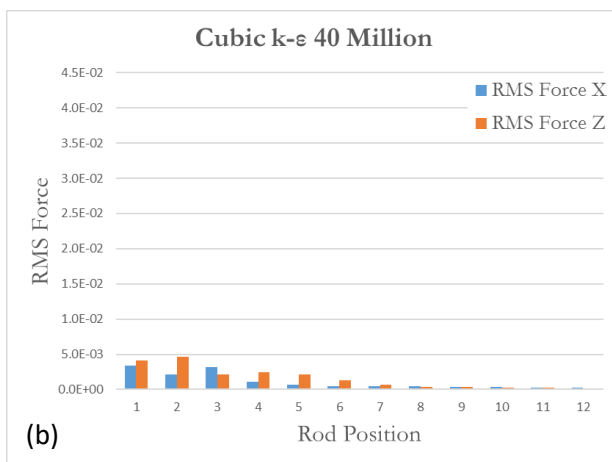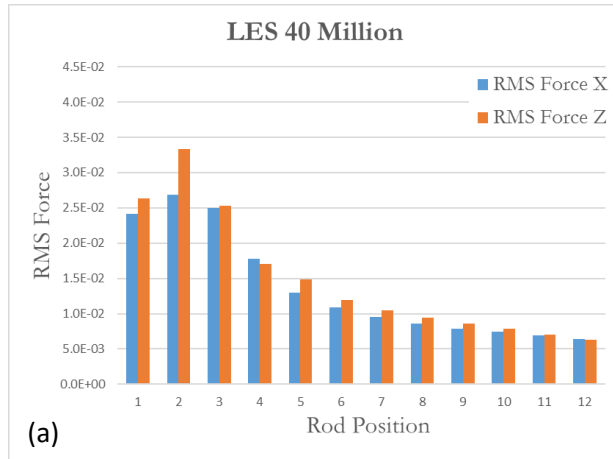
Figure 5.3.2 Predicted RMS Forces of different turbulence models along rod segments: (a) LES fine mesh, (b) Cubic k-ε fine mesh, (c) Cubic k-ε coarse mesh, (d) STRUCT fine mesh, (e) STRUCT coarse mesh.

Here we rather concentrate on providing guidelines for the specific application to GTRF, where the model generality can be replaced by strict application guidelines. The parameter f_r controls the amount of the coherent structures that are identified for model activation. A sensitivity study performed for this work indicates that the RMS force predictions are relatively insensitive to this parameter with the stipulation that the most energetic of the eddy structures must activate the STRUCT model. Although this parameter is dimensional, there is only a small difference in the prediction of $|\overline{\overline{II}}|$ throughout the domain for the fine and the coarse meshes. For this work a f_r value of 540 is used.

The parameter ϕ controls the amount by which the eddy viscosity is reduced in the activation regions, and again the parameter can vary by orders of magnitude while having a small impact on the prediction of the forces. However, there is significant physical difference between the fine and coarse mesh for the optimal value of ϕ, and even a difference in the optimal parameter for the X and Z directions. In the coarse mesh an optimal value for ϕ given a constant f_r is approximately 3e-5. This is the result shown in Figure 5.3.2.

The optimal value for the prediction of the X direction RMS forces for the 40 million cell mesh is very close to 3e-5, which is that shown in Figure 5.3.3. As it can be seen, the X direction RMS force prediction with this parameter is within approximately 5% of the LES prediction, surpassing the coarse STRUCT model with ϕ = 3e-5, and ϕ = 0.03 – as expected. However, this is a non-optimal value for the Z direction RMS force prediction. If the value of 0.03 is used instead, the z-prediction of the RMS force is improved, while the accuracy of the X-prediction of the RMS force is decreased significantly.
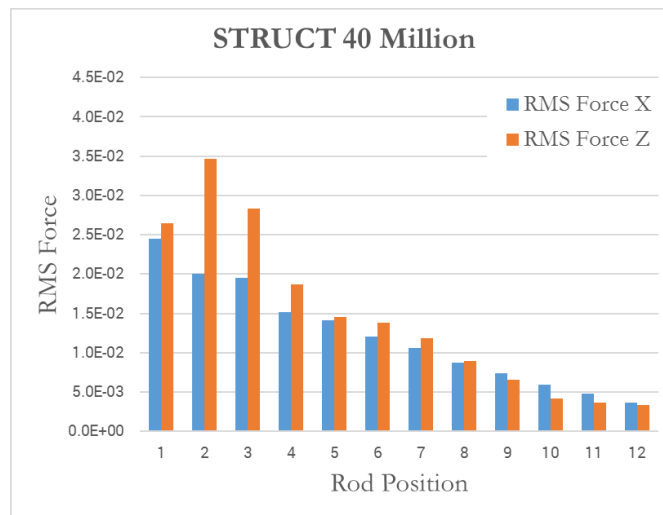
Figure 5.3.3 Fine mesh STRUCT model prediction of RMS force when using ϕ = 0.03

These results are consistent with an understanding of hybrid turbulence modeling. For the cases where ϕ = 3e-5, almost no small scale turbulence is modeled, effectively increasing the energy of the coherent structures where the model is activated. For the 40 million cell STRUCT model, this value is appropriate for the X-direction predictions, while inappropriate for the Z-direction forces. For the

coarse STRUCT simulation this value causes an overprediction of RMS force at rod segments 4-6 – by overpredicting the coherence of the structures through time.

These results indicate the importance of the handling of turbulent coherent structures in simulation, and show that a separate treatment of these structures from incoherent turbulence can signficantly improve understanding. However,the lack of an optimal value for both the X and Z directions for the fine simulation also indicates a limitation in the open STRUCT model tested in this work, and should be further evaluated.

5.3.1 Further Discussion

The success of the STRUCT turbulence model in predicting the fluctuating forces for the GTRF test case is strongly dependent on the impact of coherent structures on the rod forces. Let us now discuss further the coherent structures in the PWR subassembly.

As previously mentioned, the Q-criterion is a common parameter described by Equation 3.27 for educing turbulent coherent structures. It is theorized in this work that these coherent structures are the root cause of the fluctuating forces felt by fuel rods in pressurized water reactors. Of the models tested in this work, the fine mesh LES model is most suited for detection of the structures. This is due to the inherent strength of LES which is that most of the turbulence in the domain is directly resolved through the filtered equations. On the other hand, URANS is poorly suited for this task since the effect of turbulence everywhere is modeled through the averaged equations. Hybrid turbulence models such as STRUCT have an intermediate ability to detect such structures, still relying on URANS based equations but introducing increased resolution through reduced eddy viscosity. The central goal of this thesis is to show that the performance of the STRUCT model on coarse URANS style grids has substantial advantages in accuracy over traditional URANS models. The prediction of such coherent structures by the tested models is shown in Figure 5.3.4.
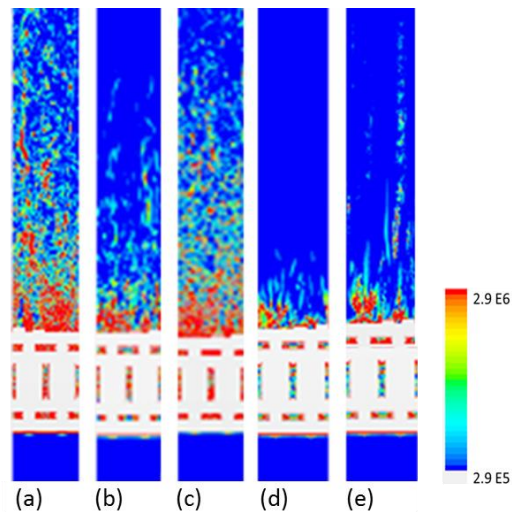

Figure 5.3.4 Figures of coherent structure prediction at a slice through the domain for (a) fine mesh LES, (b) coarse STRUCT, (c) fine STRUCT, (d) coarse cubic k-ε, and (e) fine cubic k-ε. It can be

seen that the fine mesh STRUCT model most closely matches that of the fine mesh LES model, while the coarse STRUCT predicts more structures than either the coarse or fine cubic k-ε model.
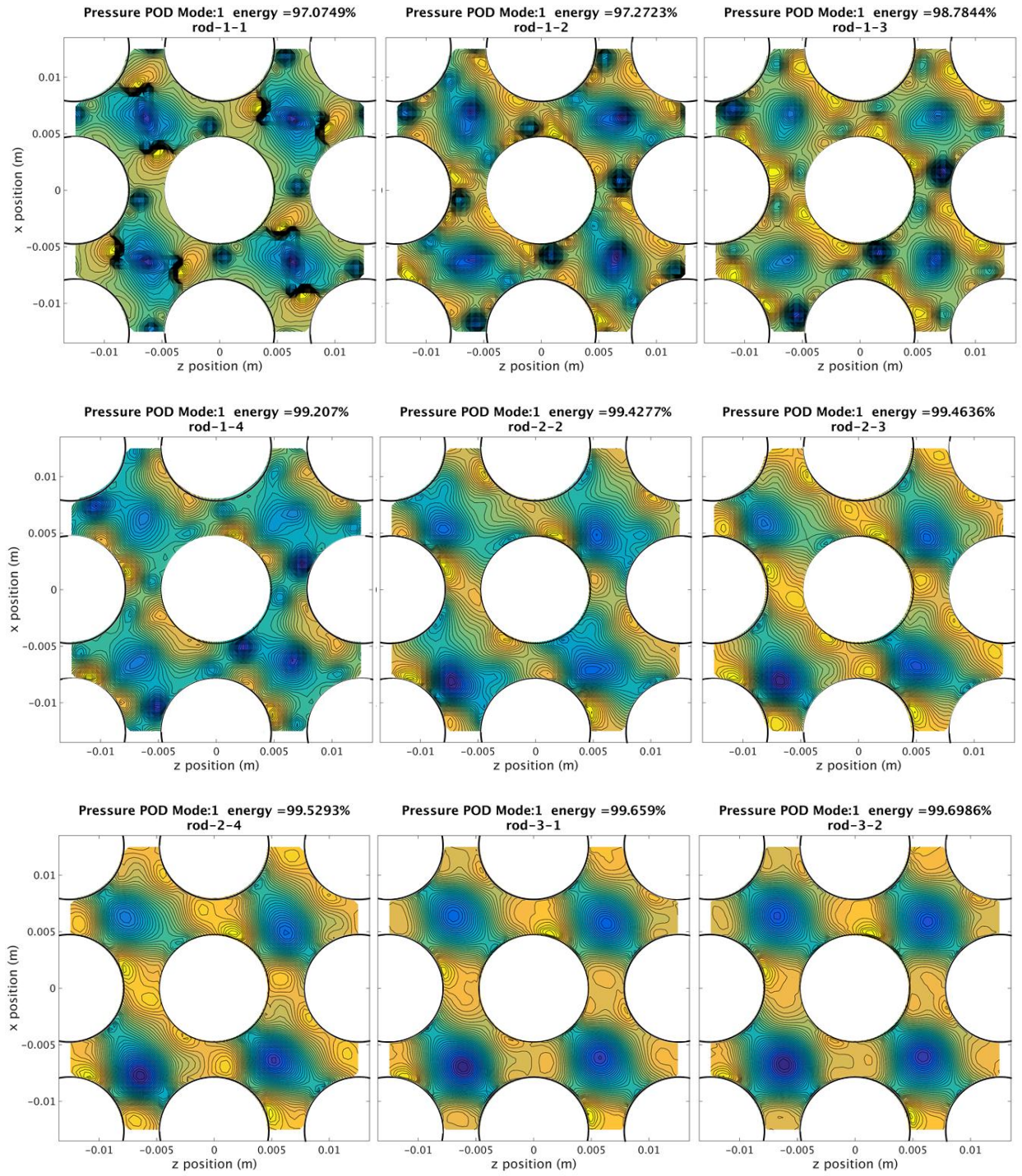
The large scale structures are generated by the spacer grid and the mixing vanes and are transported through the domain, interacting most strongly with the rods along heights 2 and 3. This can be observed in Figure 5.3.2.

A traditional method to discern underlying features in the flow is through a Fourier Fast Transform (FFT) analysis. A classical success of this application for coherent structure eduction is in the detection of the shedding frequency in simple flows past an obstruction. However, such an approach can be limited in applicability for detection of coherent structures in a complex turbulent flow. The fourier analysis is not able to use information on the spatial coherence of the flow patterns, relying instead on only a time history. An excellent discussion of the limitations of the fourier analysis for detection of coherent structures and other wavelet functions can be found in Van den Berg (2004). Elmahdi et al. (2011) reported selected LES FFTs of forces on rod segments, showing no dominant frequency corresponding to coherent structures. Such a result is supported by FFT analysis in this work.

As a recognition of the limitations of traditional FFT analysis, proper orthogonal decomposition (POD) has become a popular method for detection of coherent structures in turbulent flows. The proper orthogonal decomposition is an approach which calculates the eigenvalues of the autocorrelation matrix for the quantities of interest. Such a method guarantees the ordering of eigenvalue modes from most to least energetic, helping to separate mean flow behavior from small scale fluctuations. Information regarding the POD algorithm is widely available in the literature. An inhouse implementation of POD is utilized in this work.

The POD can be applied to any quantity of interest along a 2-Dimensionl domain in the flow, characterizing the modal distribution of the flow quantity. The 1st mode of the POD analysis corresponds closely to the mean flow behavior, while often showing clearer flow characteristics than time averaged mean quantities would show. In this work the 1st modes of the POD of pressure, velocity vectors, and Q-criterion are plotted. In the former two cases, the 1st mode contains over 99% of the energy of the flow, while in the latter case the energy is distributed over many modes. As such, the 2nd and 3rd mode of the POD of Q-criterion is plotted.

Figure 5.3.5 shows the 1st mode of pressure distributed along increasing elevation rod segments in the flow domain.

Pressure POD Mode:1 energy =97.0749% rod-1-1

Pressure POD Mode:1 energy =97.2723% rod-1-2

Pressure POD Mode:1 energy =98.7844% rod-1-3

Pressure POD Mode:1 energy =99.207% rod-1-4

Pressure POD Mode:1 energy =99.4277% rod-2-2

Pressure POD Mode:1 energy =99.4636% rod-2-3

Pressure POD Mode:1 energy =99.5293% rod-2-4

Pressure POD Mode:1 energy =99.659% rod-3-1

Pressure POD Mode:1 energy =99.6986% rod-3-2
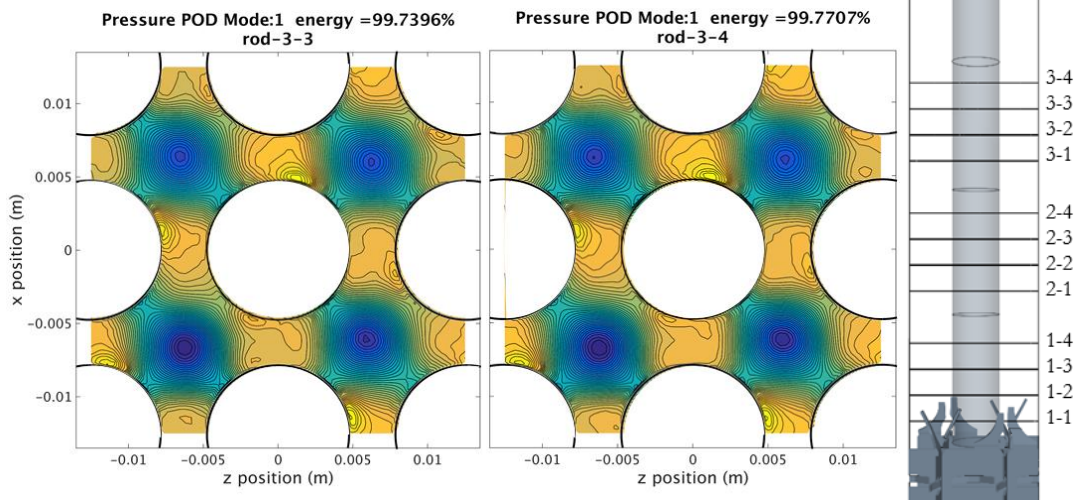
Figure 5.3.5 1st POD mode of pressure on sub-channel slices along increasing height (shown in inset).

As can be seen the pressure distribution along the lowest elevations is strongly influenced by the presence of the spacer grid, exhibiting sharp pressure gradients in the domain. These sharp gradients are slowly dissipated as the flow progresses along the domain, transitioning to the final pressure distribution along rod segment 3.

The POD distribution of the coherent structures is shown in shown in Figure 5.3.6, Figure 5.3.7, and Figure 5.3.8.

Figure 5.3.6 1ˢᵗ, 2ⁿᵈ, and 3ʳᵈ POD modes of Q-criterion along sub-channel slices along rod segment 1.
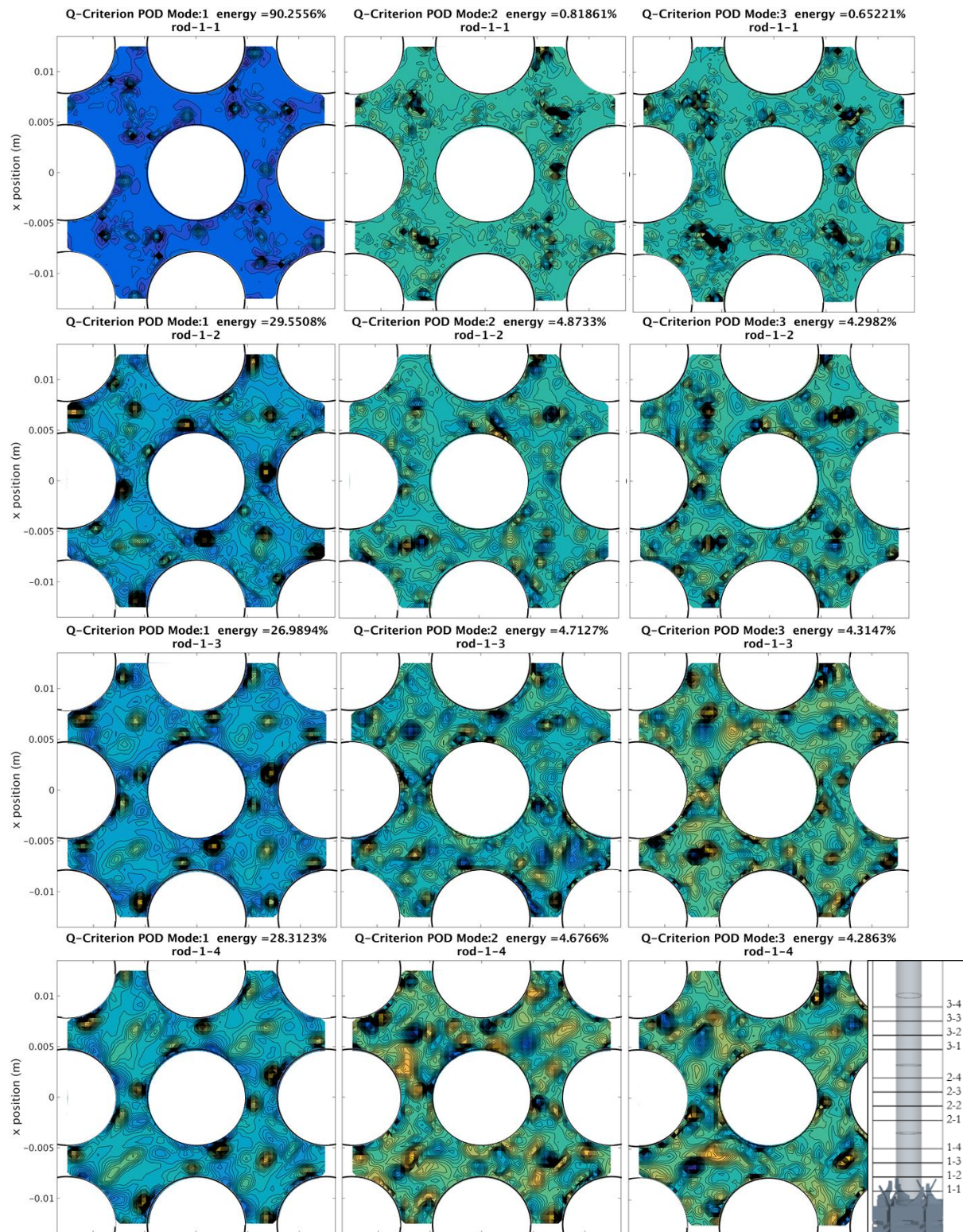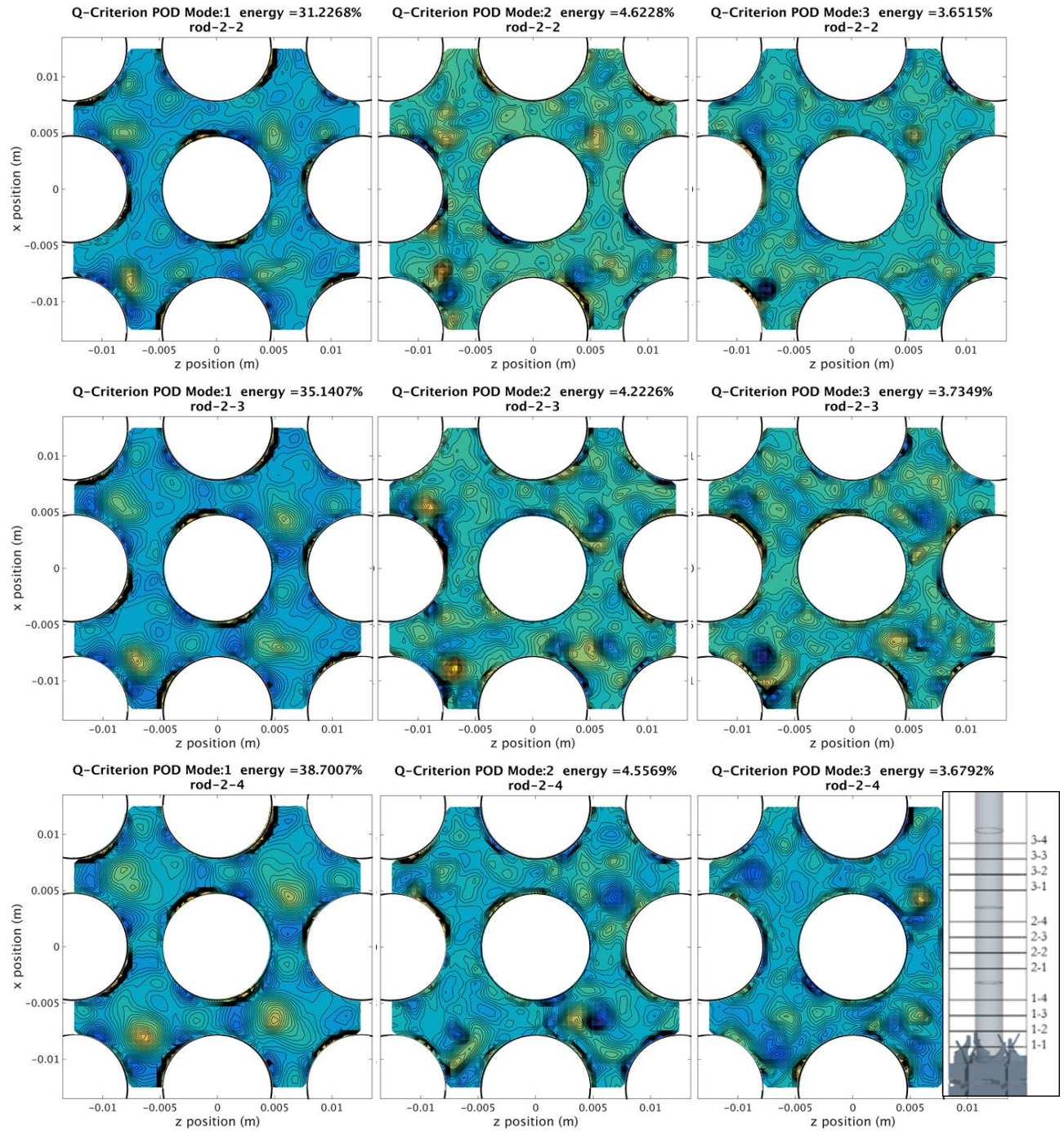
Figure 5.3.7 1st, 2nd, and 3rd POD modes of Q-criterion along sub-channel slices along rod segment 2.
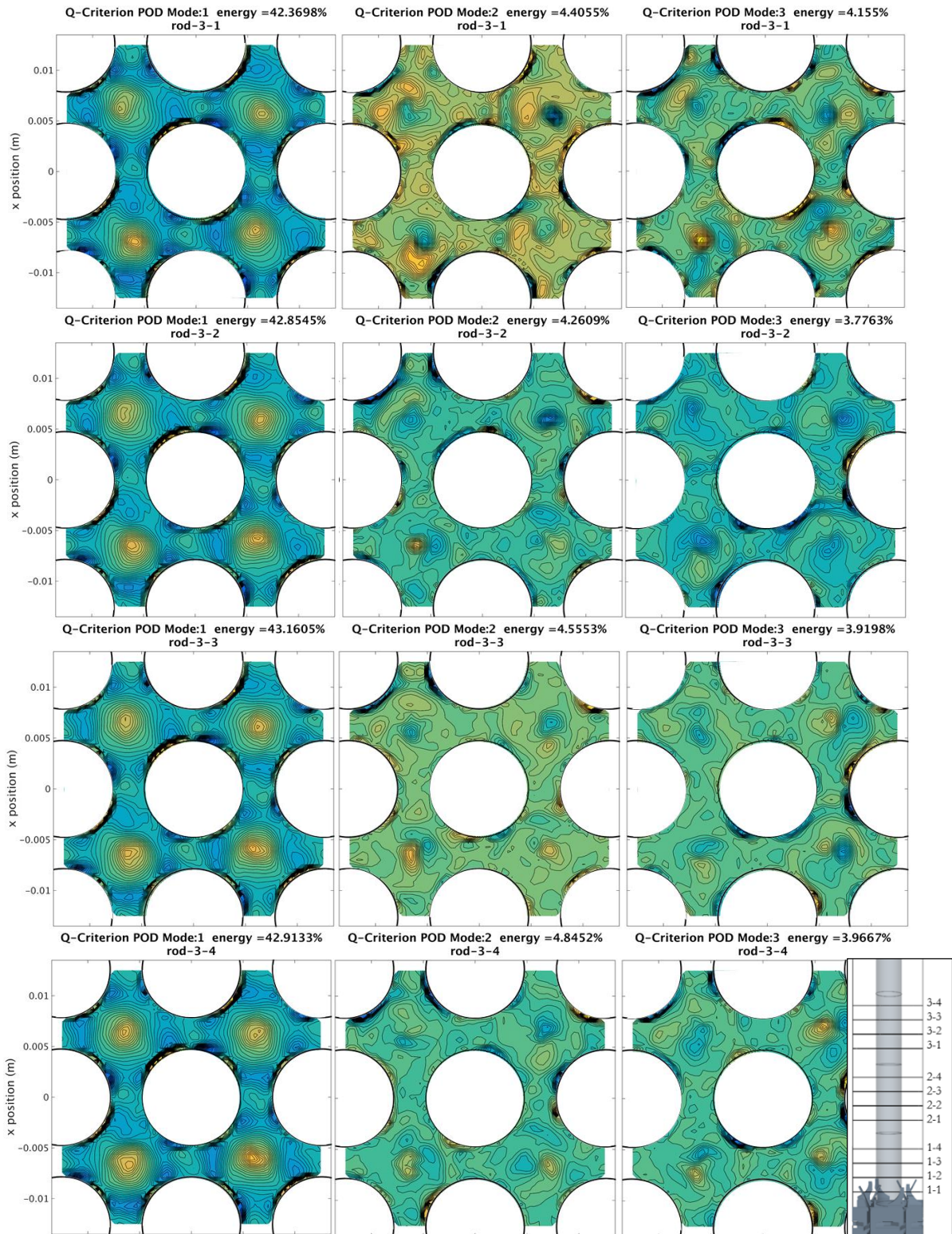
Figure 5.3.8 1st, 2nd, and 3rd POD modes of Q-criterion along sub-channel slices along rod segment 3.

As can be seen, the coherent structure distribution is very chaotic at the lowest elevations, exhibiting extremely sharp gradients due to the influence of the spacer grid and mixing vanes. Along rod segment 2, where the highest RMS force is felt, the coherent structures begin to dissipate into larger structures, and the higher modes of the Q-criterion show greater divergence in spatial distribution. Along rod segment 3, the structures begin to form into even larger structures, and their movement takes on a more steady behavior in time. This can be seen by the relatively stationary positions of the higher modes of Q-criterion along the higher rod segments.

The distribution of coherent structures is critical to understanding the pressure distribution in the subchannels. As shown in Equation 3.27, the Q-criterion represents the balance between resolved strain and shear rate. Such a balance directly impacts the pressure of the flow inside locations of extremely high or low values of the Q-criterion. Following Lenci (2016) and Lesieur and Mankbadi (1988) the relation between Pressure and $\overline{II}$ can written as a Poisson equation as:

$$\frac{1}{2\rho}\nabla^2 P = II$$

5.1

Therefore it is evident that coherent structures directly impact the pressure field in the flow, and can cause pressure forces along the rod segments. Hence it is clear that the RMS force distribution along the rod segments can be explained by the distribution of coherent structures which have a pseudo-random behavior in the flow, impacting the rod segments in a time varying manner. The peak of RMS force at rod segment 2 is clearly explained by the combination of high numbers of coherent structures as shown in Figure 5.3.4 and the high degree of mobility of these structures as shown in the POD of Q-criterion along the higher modes in rod section 2. A structure resolving approach is critical to capturing these fluctuating forces.

Finally, the velocity vector distribution is shown in Figure 5.3.9, comparing favorably to the verified flow distributions of Elmahdi et al. (2011).
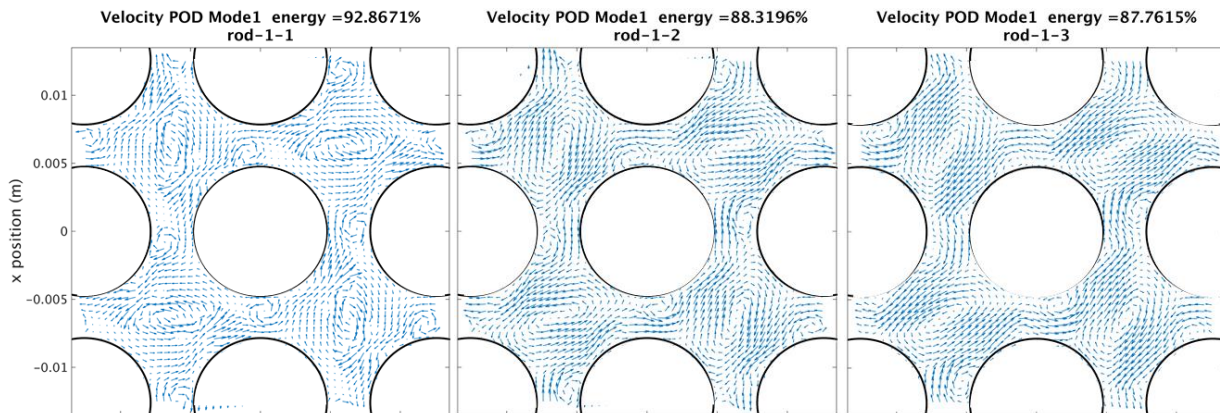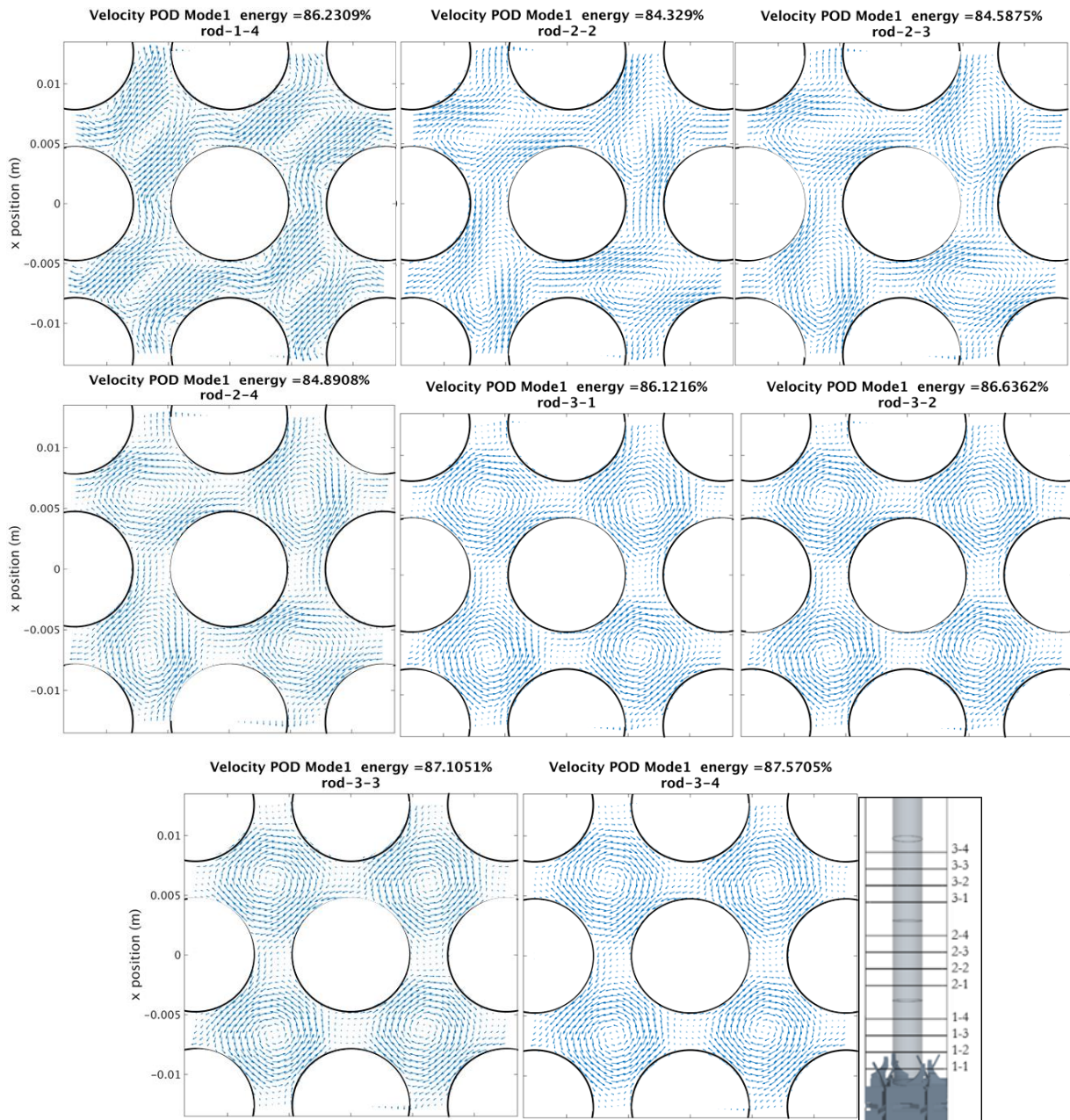
Figure 5.3.9 1st POD modes of tangential velocity vector distribution along sub-channel slices along increasing rod segment elevations.

6   Argonne National Laboratory MAX Facility Test Case

The final test case selected for this work is the MAX facility experiment that is hosted by Argonne National Laboratory.

6.1   Description

As discussed in Section 2, the experiment consists of two hexagonal inlet jets of air mixing in a large mixing tank.   The measurements are performed using particle image velocimetry for velocity measurements and an infrared camera for temperature measurements. The details of the experimental techniques are described thoroughly in Lomperski et al. (2009). Additional details regarding the inlet boundary conditions and flow conditioners can be found in Lomperski and Pointer (2015).   The experiment was conceived as a validation tool for CFD codes in studying thermal striping in SFRs and GFRs. This experiment was chosen as a representative test case since it represents the state-of-the-art in thermal striping experimental configurations in terms of accuracy and resolution.   The experimental configuration can be seen in Figure 6.1.1.
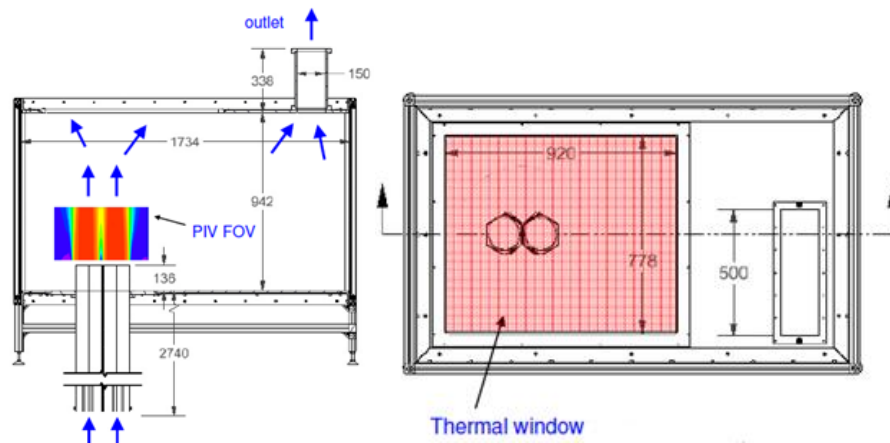

Figure 6.1.1 ANL MAX facility experimental geometry. Taken from (Lomperski et al., 2012)

In the hexagonal inlets, the flow first passes through a series of honeycomb shaped flow conditioners and wire meshes to control the turbulence levels and length scales. These structures can be seen in Figure 6.1.2.
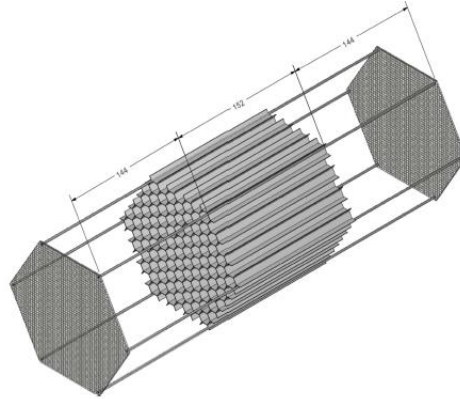
Figure 6.1.2 Hexagonal flow conditioners located in the inlet pipes. Taken from (Lomperski and Pointer, 2015)

6.2 Previous Work

At the time of writing the MAX facility was completing experimental measurements. As such the data encompassed a limited physical domain and apart from the work presented here there has been only internal CFD simulations of the experiment.

CFD simulations were used iteratively in support of the design and evaluation process. Pointer et al. (2009) leveraged LES and RANS simulations to predict the velocity, temperature, and turbulent kinetic energy distributions in the mixing tank, and to evaluate the stability of the inlet jets. A preliminary study of the impact of meshing strategies was also performed. Merzari and Pointer (2010) performed additional LES and URANS simulations to determine the effect of inlet piping extrusion into the tank, and recommended changes to the experimental configuration to increase this extrusion length.

6.3 Simulation Setup and Computational Details

All simulations were performed with the commercial finite volume CFD code STAR-CCM+ version 10.06.010. As before, the pressure-velocity coupling was performed with a segregated flow solver using the SIMPLE algorithm with 8 inner iterations. The segregated fluid temperature approach was used, with all parameters evaluated at 300 K. It is important to note that future experimental configurations are planned which exhibit a temperature difference between the inlet jets, but since the experiment is still in a testing phase only results for the isothermal cases are considered. As with all other simulations performed in this work, all URANS based methods utilized a 2nd order upwinding method with Venkatakrishnan gradient limiters for calculating the interpolation of convective fluxes; the LES method utilized a BCD technique.

All simulations were performed in unsteady mode, with a second order implicit temporal discretization, using a timesetp to ensure a courant number below 1. The simulation was performed for 100s, with statistics being collected at 10 seconds at which time the physical variables reached an unsteady convergence. A figure of the simulation geometry is shown in Figure 6.3.1.
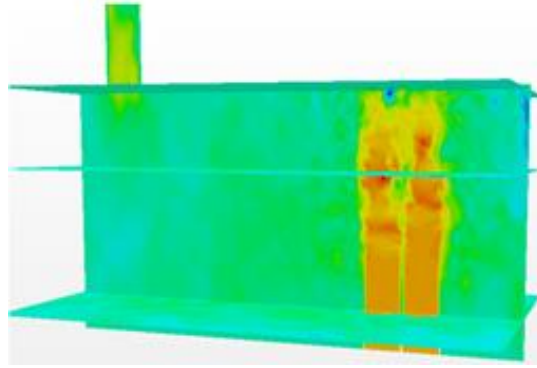
Figure 6.3.1 Computational domain for the ANL MAX facility experiment.

The boundary conditions set for this simulation was no-slip walls everywhere except for the two hexagonal velocity inlets and a singular pressure outlet boundary condition at the exit chimney.

At the time of writing, the experimental data is limited to a small domain near the inlet of the mixing tank and at the top measurement plane as well. This domain is depicted in Figure 6.3.2.
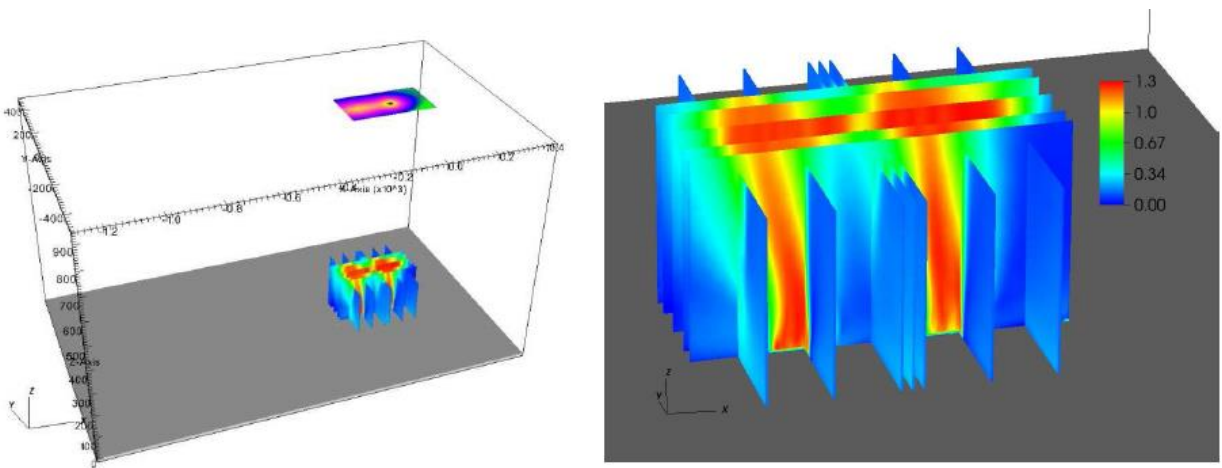
Figure 6.3.2 Measurement planes in the mixing tank.

For the present work, experimental comparisons are made along the X-Z plane at Y=0. Further experimental measurements are expected to be forthcoming.

In this simulation, particular care must be taken to ensure that inlet velocity and turbulence levels match those of the experiment. Such a concern is necessitated by the use of hexagonal inlet pipes and honeycomb flow conditioners. The experimentally measured time averaged velocity profile 20mm above the inlet as reported in (Lomperski et al., 2009) is shown in Figure 6.3.3.
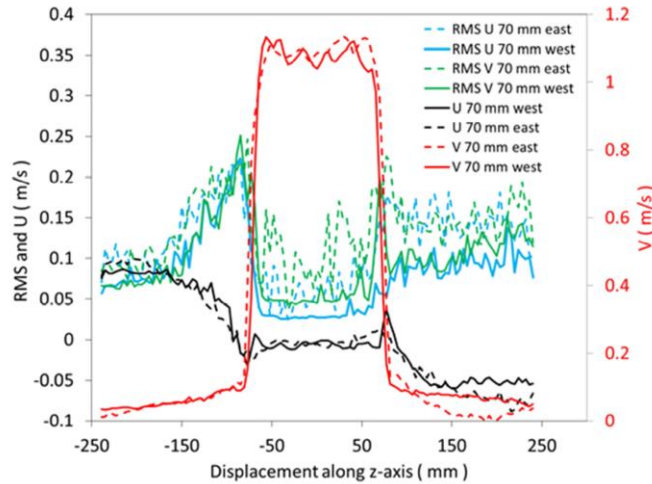
Figure 6.3.3 Mean and RMS velocity profiles on the midline 20 mm above inlets, view from side of the tank. Taken from (Lomperski and Pointer, 2015)

It is clear that the inlet profile is not a standard fully developed profile, and additionally it is not clear what the appropriate turbulence quantities are since they have not been directly measured in the experiment.

It is also expected that the instantaneous profiles at the inlet boundary should exhibit more drastic peaking of the velocity profiles due to the honeycomb conditioner. The following vertical velocity profile was specified at the inlet based on the x and y position as:

$$U = 0.95 + 0.15|(sin(256x - 3.2)| + 0.15|sin(256y - 3.2)| \qquad 6.1$$

Such a form replicates the expected peaking between the honeycomb walls, which can be seen in Figure 6.3.4. Zero lateral velocity was specified at the inlet.
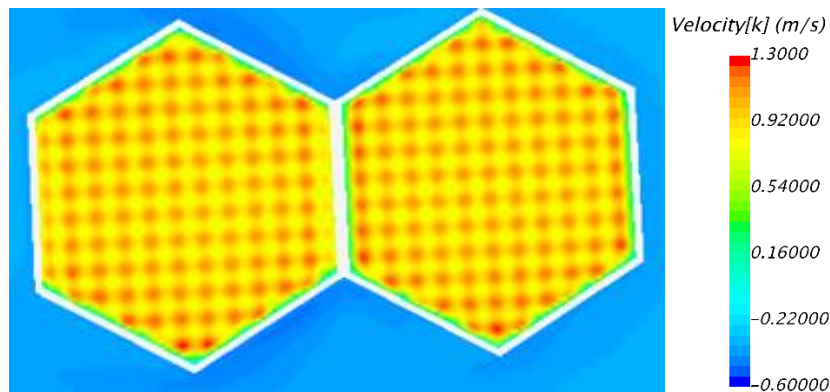
Figure 6.3.4 Inlet velocity profile specified

The turbulent intensity levels and velocity magnitudes were calibrated to match the downstream profiles as closely as possible with that of the experiment. The ideal turbulent intensity was

determined as 0.005, along with a turbulent viscosity ratio of 10. For LES a turbulent length scale of 6.4mm was set, which was determined by the spacing of the honeycomb conditioner.

The following figures show the degree to which the simulation is in agreement with the experimental measurements.
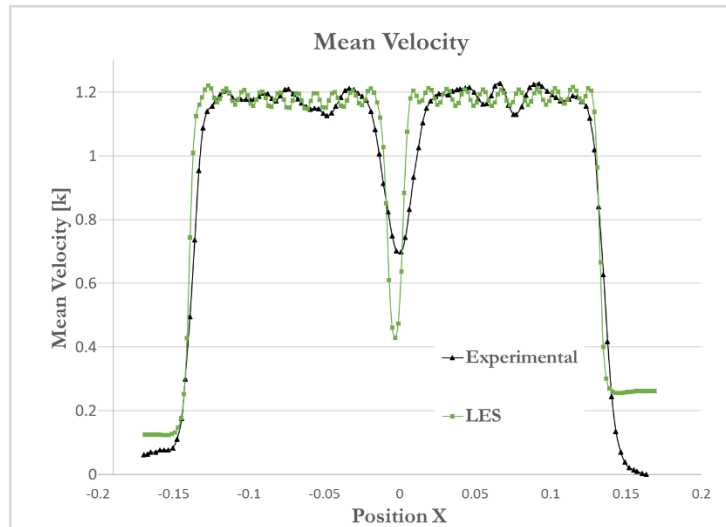
Figure 6.3.5 Experimental and LES mean velocity profiles, 20 mm above the inlets.

Of notable difference is the increased velocity experimentally measured between the jets as compared to the LES predictions. Such a discrepancy is believed to be due to an incomplete description of the inlet profiles and error in mixing predictions. The LES model predicts a slight degree of recirculation near the right jet inlet.
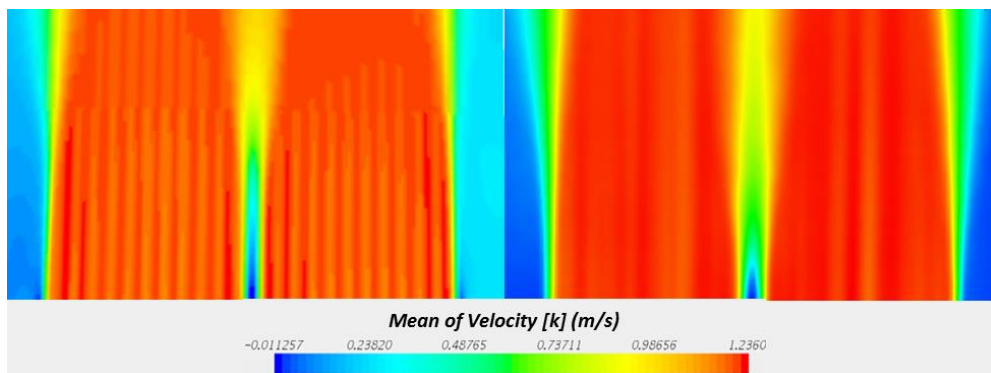
Figure 6.3.6 LES (left) and experimental (right) figure of the mean velocity along the PIV data plane.

RMS Velocity [k]

| 0.0000 | 0.044040 | 0.088080 | 0.13212 | 0.17616 | 0.22020 |
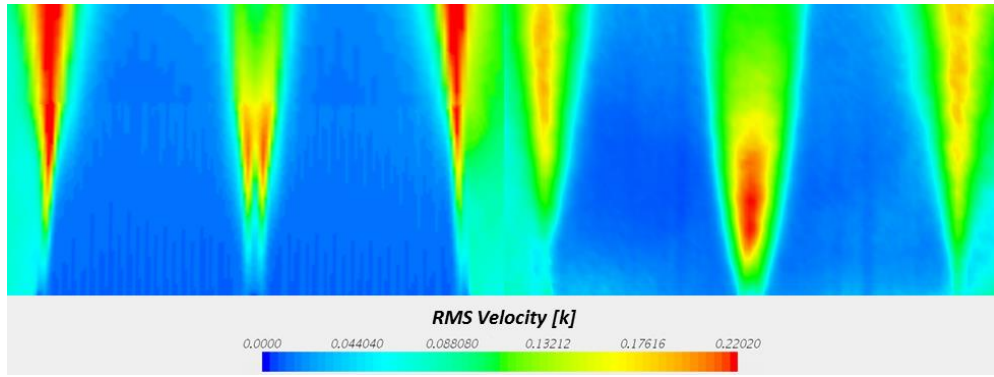
Figure 6.3.7 LES (left) and experimental (right) figure of the RMS velocity along the PIV data plane.

These preliminary results suggest the acceptability of the imposed simulation setup for the following models, including the initial and boundary conditions.

6.3.1   Meshing Strategy

The computational domain was meshed with isotropic hexahedral cells of varying sizes of 2mm, 4mm, 8mm, and 16mm. This strategy was utilized due to the very large geometric domain of the experiment. Near the inlet extrusion region, the cell size was 2mm and grew steadily to the 16mm mesh. A 2 cell prism layer of 4mm with a growth rate of 1 was used at the top of the domain and disabled everywhere else. The cell size was ensured to respect wall $y+ > 30$ everywhere in the domain. The computational mesh used in this study is shown in Figure 6.3.8
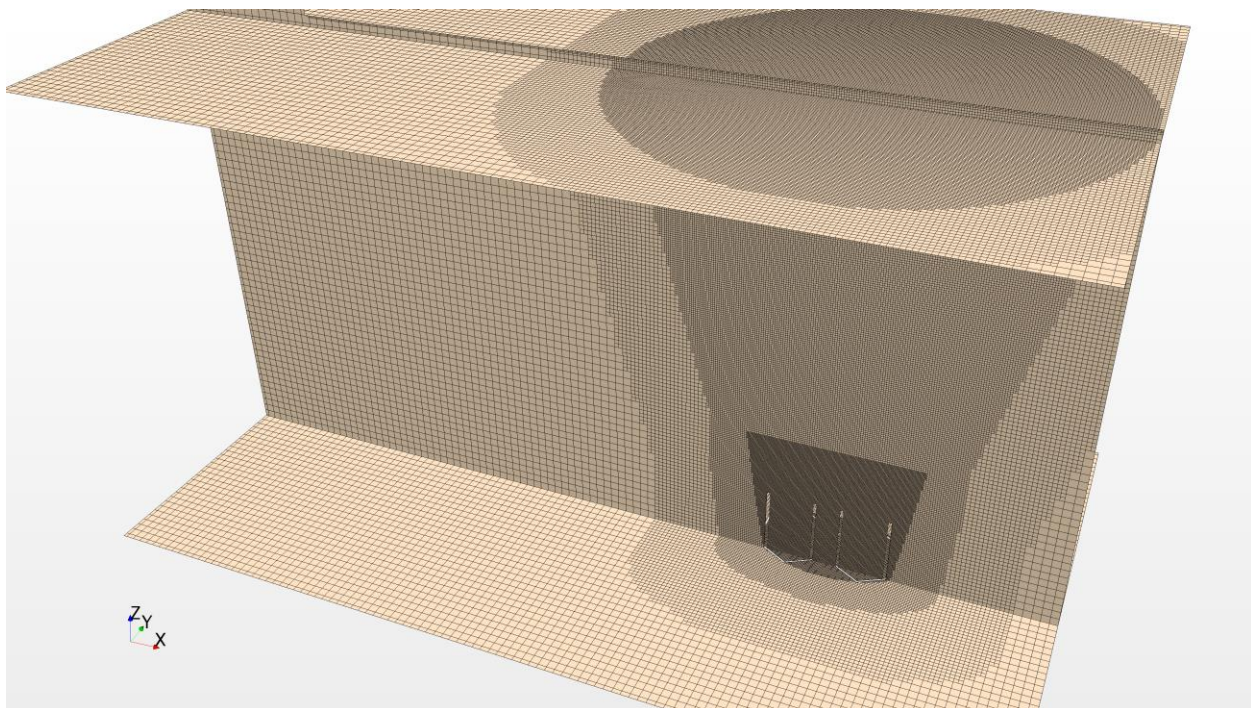
Figure 6.3.8 Computational mesh used for all simulations, showing a gradual refinement surrounding the inlet jets.

6.4 Results

Due to the lack of complete experimental data the turbulence models are first evaluated at the experimental available data plane. As it will be shown, the LES model most closely matches that of the experimental data, and will be used as a reference solution for discussing the behavior of the models outside of the experimental domain.

Both the STRUCT and Cubic k-ε turbulence model was tested alongside the LES model and in comparison to experimental data. For the STRUCT model the values for the controlled parameters of ϕ and f_r were set as 0.01 and 6.

6.4.1 Experimental Comparison

As discussed in Section 6.3 the matching of experimental data at the data planes near the inlet of the tank is heavily dependent on the inlet conditions specified at the boundary, and it was shown that the LES model with the specified inlet conditions was able to closely match the experimental data at such elevations. Furthermore, both the STRUCT and cubic k-ε models are able to approximately reproduce these profiles for the mean velocity, which can be seen in Figure 6.4.1.

Figure 6.4.1 Mean velocity predictions along the PIV data plane: (a) experimental, (b) LES, (c) STRUCT, (d) Cubic k-ε

It was shown in Figure 6.3.7 that there is a close agreement between the LES result and the experimental data while it is shown in Figure 6.4.2 that the STRUCT model closely matches that of the experimental data and the LES, while over predicting the RMS velocity at the edges of the jet. The cubic k-ε model under predicts the RMS velocity at all locations, especially in the center of the jets, which is to be expected based on the overproduction of eddy viscosity as seen in the previous two

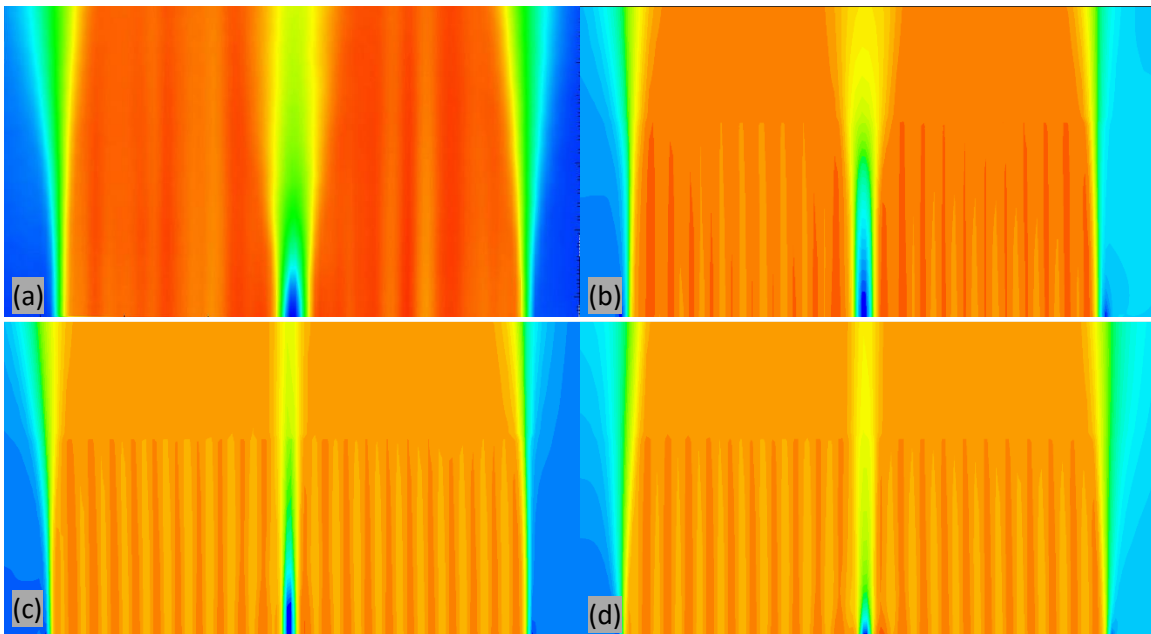test cases. All models under predict the mixing between the two jets, with the LES model predicting this mixing most accurately.
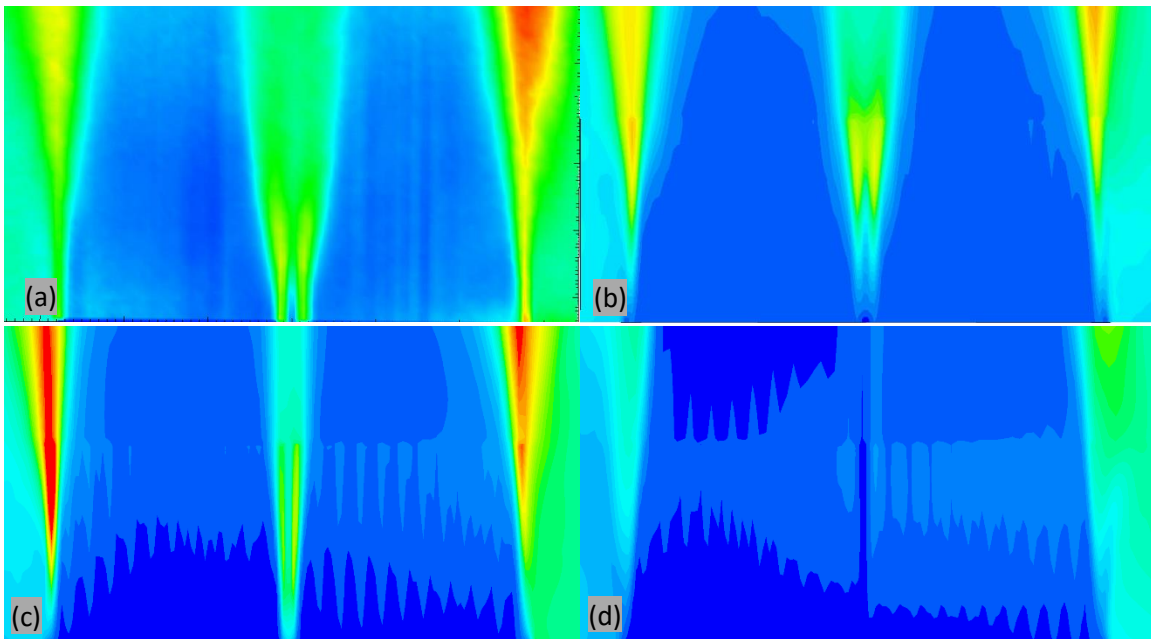
Figure 6.4.2 RMS velocity predictions along the PIV data plane: (a) experimental, (b) LES, (c) STRUCT, (d) Cubic k-ε

Profiles of the RMS velocity and mean velocity are shown in the following Figure 6.4.4 and Figure 6.4.3 respectively. As can be seen in Figure 6.4.3 the mean velocity profiles are reasonably well predicted at the first three elevations, which can be expected since the effect of inlet velocity specification is dominant at these elevations. A difference in the peaking of the profiles at the jets can be observed, and this is due to the simplification of the inlet profiles in Equation 6.1 as a simple sin and cos function. In reality the velocity peaking is non uniform. Such a difference in the peaking can be assumed to have an effect on the RMS velocity predictions as well.
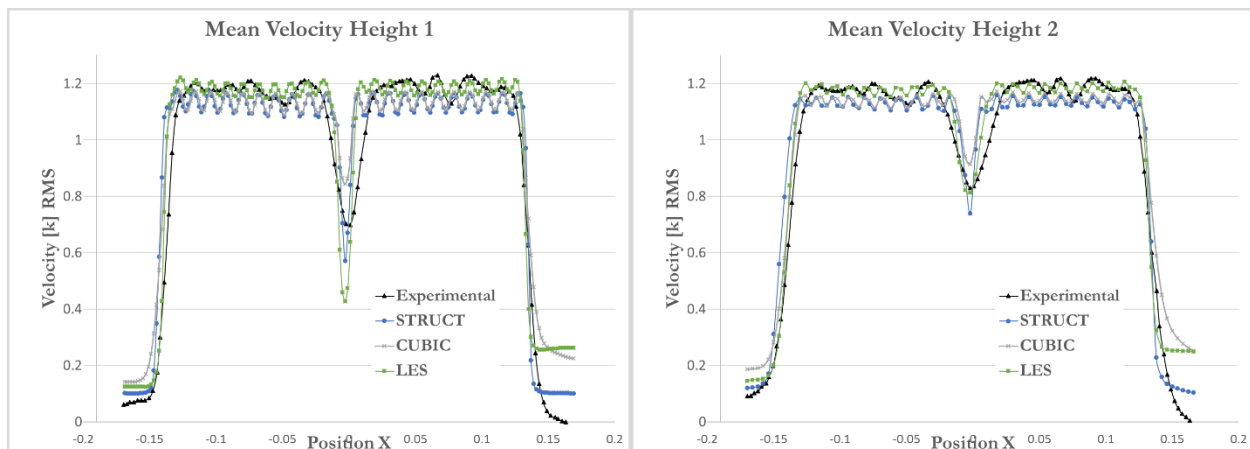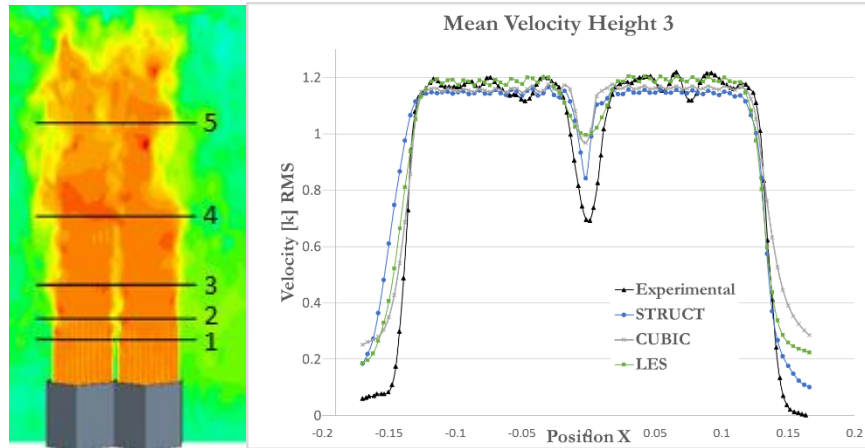
Figure 6.4.3 Profiles of the mean velocity along the heights shown in the inset.

As it can be seen in the plots for the RMS velocity, the STRUCT and LES models closely match the experimental data, while predicting a narrower peaking of RMS velocity between the jets than is experimentally measured. The cubic RMS velocity predictions are under predicted at all locations and heights. At the third elevation, the LES model predicts closely the spread in RMS velocity at the center of the jets, while the STRUCT model remains narrowly peaked.

Figure 6.4.4 Profiles of the RMS Velocity along the heights shown in the inset.

Furthermore the FOM introduced in Section 4, and following Equation 4.2 – where the FOM is now normalized by the cubic k-ε model, is utilized for the mean and RMS velocity fields. As it can be seen in **Table 6.4.1** the STRUCT model shows a slightly worse performance for the mean velocity field, but maintains an equal performance to the LES model in predicting the RMS velocity fields.
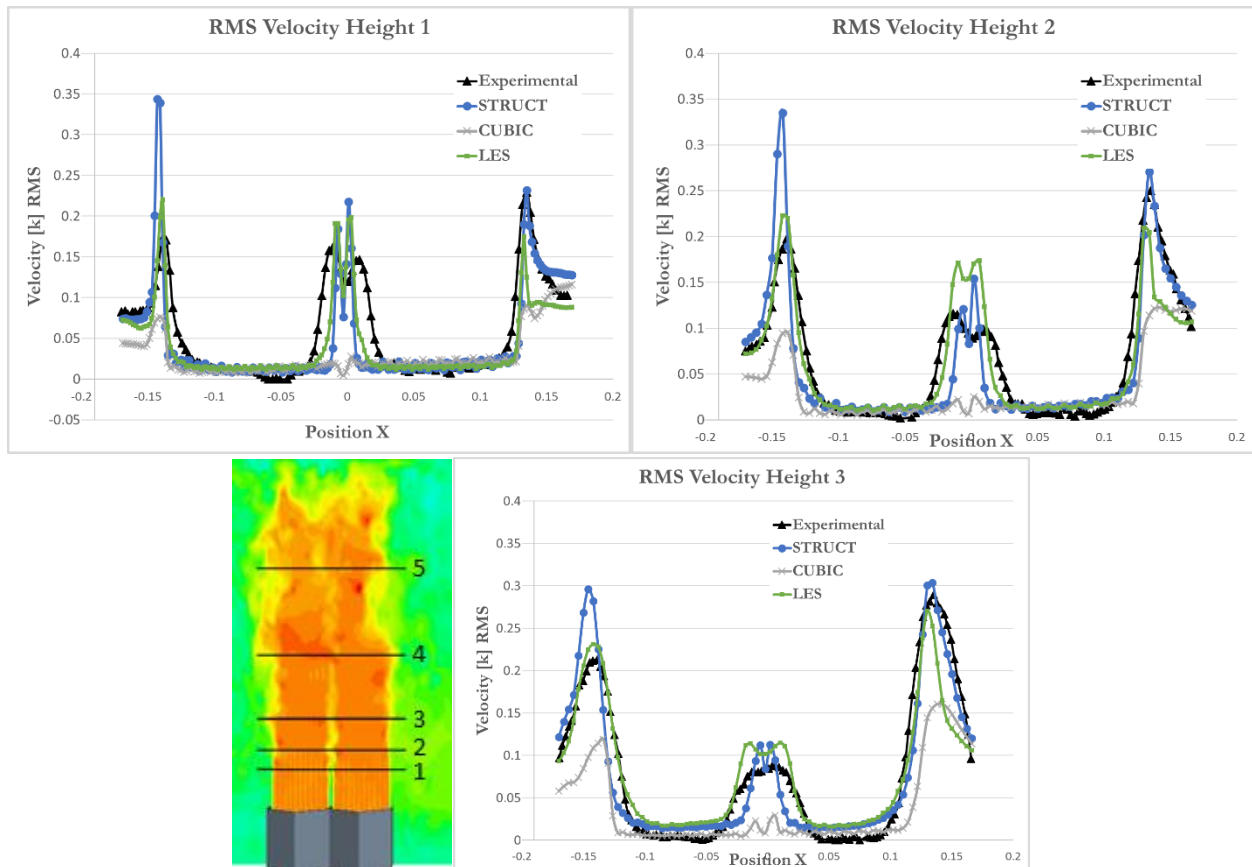
	Mean Velocity	**RMS Velocity**
Cubic k-ɛ	1.00	1.00
LES	0.71	0.23
STRUCT	1.11	0.23

Table 6.4.1. Figure of Merit of the tested models for the mean and RMS velocity fields.

6.4.2   *Full Domain Comparison and STRUCT Activation*

The experimental domain at the present state is limited to the regions discussed in the previous sections, however, it is useful to discuss the performance of the models in the full computational domain.

In the full computational domain, all models predict maximum variation at an elevated location on the right side of the jets. This value is over predicted for the STRUCT model, indicating that a non-optimal value for ϕ was set in this location. As with the experimental domain, the Cubic k-ɛ model underpredicts the RMS velocity at all locations and by a large degree. In addition, the STRUCT model shows improved perfomance in the recirculation region near the rightmost wall and at the impingement location as well.
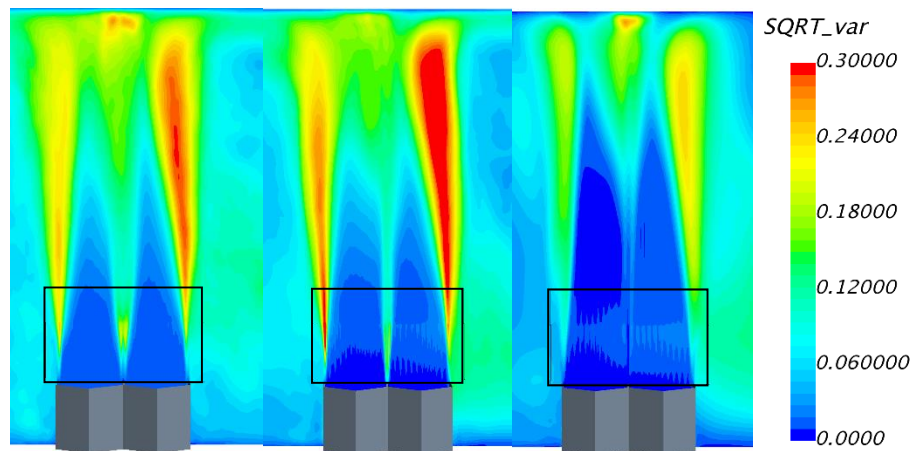
Figure 6.4.5 Full domain RMS velocity predictions with LES (left), STRUCT (center), and Cubic k-ɛ (right). The experimental domain is shown as the black outline.

The behavior of the models can be qualitatively discussed by inspection of the instantaneous velocity, shown in Figure 6.4.6. The LES model predicts a wide range of eddy scales and shows a fluctuating region at the lowest elevations in addition to the mixing region. The cubic k-ɛ model

predicts an instantaneous velocity profile similar to an averaged profile, which is as expected, and shows no prediction of eddies – instead transitioning smoothly from regions of high to low velocity. The STRUCT model can be seen to predict large scale eddies while smoothing out fluctuations present in the lower elevations. As can be seen in Figure 6.4.6, as well as the plots of RMS velocity, the mixing between the two jets at the lowest elevation is under predicted in comparison to the experimental and LES results – indicating a non-optimal value for ϕ or f_r in these regions.
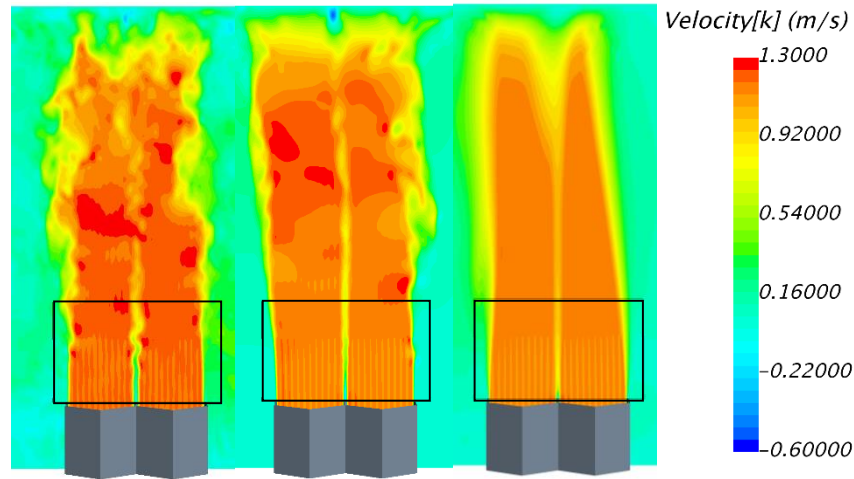
Figure 6.4.6 Full domain predictions of instantaneous velocity profiles for LES (left), STRUCT (center) and Cubic k-ε (right). The experimental domain is shown as the black outline.

Figure 6.4.7 shows the RMS Velocity at the elevations outside of the experimental domain, showing a continued trend of close agreement between LES and STRUCT with the cubic k-ε model predicting a too low RMS velocity at all locations.
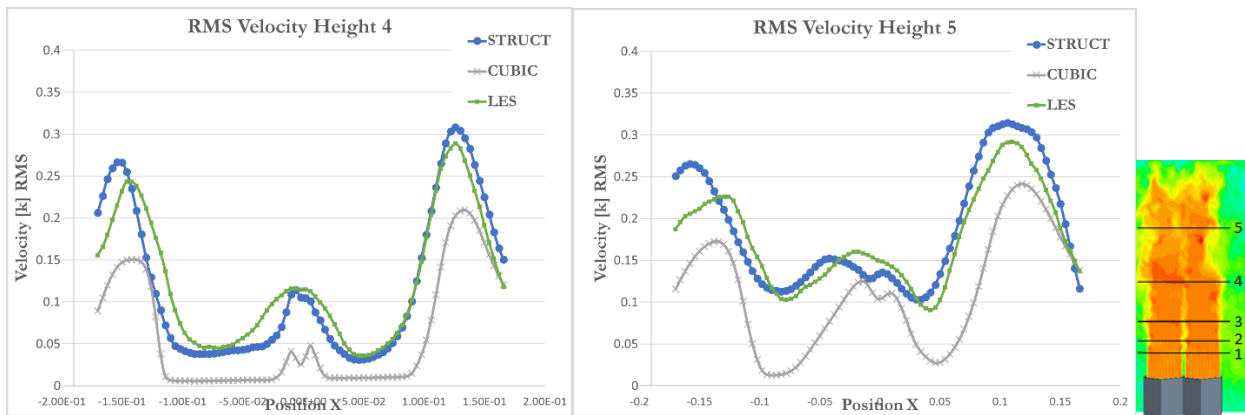
Figure 6.4.7 Plots of RMS velocity at the 4th and 5th elevation (shown in the inset), which is outside the experimental domain.

The following Figure 6.4.8 shows the region of STRUCT model activation (blue) with the model activating in the regions between and on the edges of the two jets, corresponding to regions of high RMS velocity and subsequently high coherent structure regions.
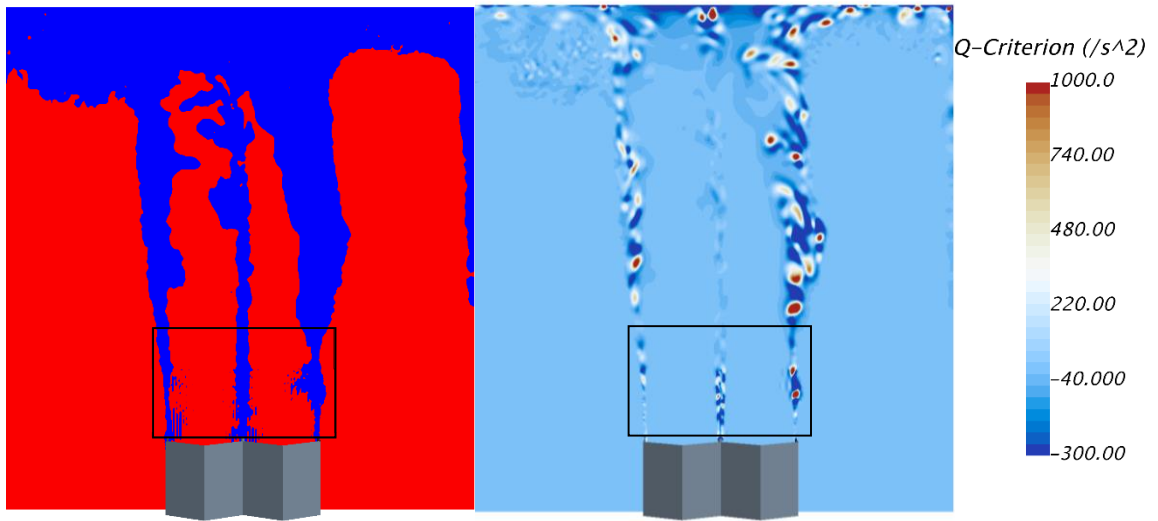
Figure 6.4.8 STRUCT model activation in blue (left) and coherent structure plot (right)

These results must be verified as more experimental data becomes available in the future.

7 Conclusion

The complexity of simulating complex inherently unsteady flow phenomena typical Nuclear Engineering applications has been investigated on three relevant experimental test cases: the JAEA parallel triple jet, a PWR mixing vane flow, and the twin jet experiment at the ANL MAX facility. It is shown that in such test cases, the resolution of turbulent structures is critical for the understanding and prediction of mean and varying flow parameters. The performance of LES, traditional URANS models, and finally the recently developed STRUCT hybrid turbulence model was evaluated on each flow case.

For the triple jet test case, the performance of the STRUCT model on a coarse URANS-like mesh was shown to be comparable to that of the LES model on a much finer grid in predicting mean and fluctuating profiles of velocity and temperature, as well as the frequencies of the fluctuations. These results were validated favorably against the experimental data of Tokuhiro and Kimura (1999).

When applied to the challenge of PWR mixing vane induced vibrations, the RMS forces along rod segments were calculated – showing the applicability of the STRUCT model on coarse meshes, matching closely with the LES predictions and that of Elmahdi et al. (2011). The impact of the prediction of coherent structures in the flow on these forces was evaluated through the use of the proper orthogonal decomposition (POD).

Finally, the predictions of the mean and varying flow parameters in the ANL MAX facility test case were compared against experimental data. In the experimentally measured domain, the impact of the inlet boundary conditions was highlighted, and the predictions of the LES and STRUCT models most closely matched that of the experiment. Further, the STRUCT and LES models showed similar flow behaviors far from the experimental domain. Additional experimental data must be collected to validate the predictions of the STRUCT and LES models for this flow case.

The good performance of the STRUCT approach on three representative test cases relevant to thermal striping flows indicates the potential of the model for industrial engineering and design applications. Furthermore, the influence of turbulent coherent structures on thermal striping flows is established. The STRUCT model accurately predicts flow quantities relevant to thermal striping applications on computational meshes much coarser than that of traditional LES models, enabling computational speedups between 20X for the triple jet test case to 50X for the PWR test case. While further testing of the robustness of the model on reactor specific geometries must be performed, the model warrants improved usage for sodium fast reactor internal flows.

References

[1]   Acton, M.J., Lenci, G., Baglietto, E., 2015. Structure-Based Resolution of Turbulence for Sodium Fast Reactor Thermal Striping Applications, in: Submitted to the 16th International Topical Meeting on Nuclear Reactor Thermal Hydraulics (NURETH-16).

[2]   Baglietto, E., Ninokata, H., 2007. Improved Turbulence Modeling for Performance Evaluation of Novel Fuel Designs. Nucl. Technol. 158, 237–248.

[3]   Baglietto, E., Ninokata, H., 2006. Anisotropic Eddy Viscosity Modeling for Application to Industrial Engineering Internal Flows. Int. J. Transp. Phenom. 8, 85–101.

[4]   Bakosi, J., Christon, M. a., Lowrie, R.B., Pritchett-Sheats, L. a., Nourgaliev, R.R., 2013. Large-eddy simulations of turbulent flow for grid-to-rod fretting in nuclear reactors. Nucl. Eng. Des. 262, 544–561. doi:10.1016/j.nucengdes.2013.06.007

[5]   Baratto, F., Bailey, S.C.C., Tavoularis, S., 2006. Measurements of frequencies and spatial correlations of coherent structures in rod bundle flows. Nucl. Eng. Des. 236, 1830–1837. doi:10.1016/j.nucengdes.2005.12.009

[6]   Benhamadouche, S., Moussou, P., Maitre, C. Le, 2009. CFD Estimation of the Flow-Induced Vibrations of a Fuel Rod Downstream a Mixing Grid, in: Proceedings of the ASME 2009 Pressure Vessels and Piping Division Conference PVP2009.

[7]   Bieder, U., Falk, F., Fauchet, G., 2015. CFD analysis of the flow in the near wake of a generic PWR mixing grid. Ann. Nucl. Energy 82, 169–178. doi:10.1016/j.anucene.2014.08.004

[8]   Brewster, R., Carpenter, C., Volpenhein, E., Smith, J., 2015. Application of CD-Adapco Best Practices to Nestor Omega MVG Benchmark Exercises Using STAR-CCM+ 640–652.

[9]   Brunings, J., 1982. LMFBR Thermal-Striping Evaluation. Canoga Park, California.

[10]   Cao, Q., Lu, D., Lv, J., 2012a. Numerical Investigation on Temperature Fluctuation of the Parallel Triple-Jet. Nucl. Eng. Des. 249, 82–89. doi:10.1016/j.nucengdes.2011.07.018

[11]   Cao, Q., Lu, D., Zhang, P., Shi, W., Tian, L., 2012b. Experimental Investigation on Effect of Inlet Velocity Ratios for 3-D Temperature Fluctuation Caused by Coaxial-Jet Flow. At. Energy Sci. Technol.

[12]   Carasik, L.B., Ruggles, A.E., Hassan, Y.A., 2014. Preliminary Investigation of Turbulent Flow Behavior of 3-D Twin Jets using CFD Analysis, in: Transactions of the American Nuclear Society, Vol. 110. Reno, Nevada.

[13]   CD-adapco, 2014. User Guide, STAR-CCM+ Version 9.04.

[14]   Chacko, S., Chung, Y.M., Choi, S.K., Nam, H.Y., Jeong, H.Y., 2011. Large-Eddy Simulation of Thermal Striping in Unsteady Non-Isothermal Triple Jet. Int. J. Heat Mass Transf. 54, 4400–4409. doi:10.1016/j.ijheatmasstransfer.2011.05.002

[15]   Chang, D., Tavoularis, S., 2008. Simulations of turbulence, heat transfer and mixing across narrow gaps between rod-bundle subchannels. Nucl. Eng. Des. 238, 109–123. doi:10.1016/j.nucengdes.2007.06.001

[16]   Conner, M.E., Baglietto, E., Elmahdi, A.M., 2010. CFD methodology and validation for single-phase flow in PWR fuel assemblies. Nucl. Eng. Des. 240, 2088–2095. doi:10.1016/j.nucengdes.2009.11.031

[17]   Crosskey, M., Ruggles, A., 2014. UTK Twin Jet Water Facility Computational Fluid Dynamics Validation Data Set, in: Proceedings of ICAPP 2014. Charlotte, NC, pp. 1940–1945.

[18]   Delafontaine, S., Ricciardi, G., 2012. Fluctuating pressure calculation induced by axial flow trough mixing grid. Nucl. Eng. Des.

[19]   Durbin, P.A., Reif, B.A., 2011. Statistical Theory and Modeling for Turbulent Flows.

[20]   Durve, A., Patwardhan, A.W., Banarjee, I., Padmakumar, G., Vaidyanathan, G., 2010. Thermal Striping in Triple Jet Flow. Nucl. Eng. Des. 240, 3421–3434. doi:10.1016/j.nucengdes.2010.07.025

[21]   Elmahdi, A., Lu, R., Conner, M., Karoutas, Z., Baglietto, E., 2011. Flow Induced Vibration Forces on a Fuel Rod by LES CFD Analysis, in: The 14th International Topical Meeting on Nuclear Reactor Thermal Hydraulics (NURETH-14).

[22]   Elmahid, A., Lu, R., Conner, M., Karoutas, Z., Baglietto, E., 2011. Flow Induced Vibration Forces on a Fuel Rod by LES CFD Analysis, in: Proceedings of the 14th International Topical Meeting on Nuclear Reactor Thermal Hydraulics (NURETH-14). Toronto, Canada, pp. 1–6.

[23]   Ferziger, J.H., Peric, M., 2002. Computational Methods for Fluid Dynamics.

[24]   Gelineau, O., Sperandio, M., 1994. Thermal Fluctuation Problems Encountered in LMFRs, in: Specialistic Meeting on "Correlation Between Material Properties and Thermohydraulics Conditions in LMFBRs." Aix-en-Provence, France.

[25]   Girimaji, S.S., Srinivasan, R., Jeong, E., 2003. PANS Turbulence model for seamless transition between RANS and LES: fixed-point analysis and preliminary results, in: Proceedings of the 4th ASME-JSME Joint Fluids Engineering Conference.

[26]   Hattori, N., Arai, Y., Sugiyama, A., Koyabu, K., Hirakawa, M., 1998. Experimental Study of Coaxial Double Pipe Air Jets at Different Temperatures. Heat Transf. - Japanese Res. 27, 431–446.

[27]   Hu, L.W., Kazimi, M.S., 2006. LES Benchmark Study of High Cycle Temperature Fluctuations Caused by Thermal Striping in a Mixing Tee. Int. J. Heat Fluid Flow 27, 54–64. doi:10.1016/j.ijheatfluidflow.2005.08.001

[28]   IAEA, 2006. Fast Reactor Database 2006 Update, IAEA-TECDOC-1531.

[29]   Ikeno, T., Kajishima, T., 2006. Decay of Swirling Turbulent Flow in Rod-bundle. J. Fluid Sci. Technol. 1, 36–47. doi:10.1299/jfst.1.36

[30]   Jayaraju, S., EMJ, K., Baglietto, E., 2010. Suitability of wall-functions in Large Eddy Simulation for thermal fatigue in a T-junction. Nucl. Eng. Des. 240.

[31]   Jung, J.H., Yoo, G.J., 2004. Analysis of Unsteady Turbulent Triple Jet Flow with Temperature Difference. J. Nucl. Sci. Technol. 41, 931–942. doi:10.1080/18811248.2004.9715567

[32]   KAERI, 2006. Experimental Study on the Thermal Striping at a Thermal Mixing Region Simulating the Outlet of a LMR Fuel Assembly.

[33]   Kawamura, T., Shiina, K., Ohtsuka, M., Tanaka, I., Hirayama, H., Tanimoto, K., Fukuda, T., Sakashita, A., Mizutani, J., 2002. Experimental Study on Thermal Striping in Mixing Tees with Hot and Cold Water, in: Proceedings of ICONE10. Arlington, VA.

[34]   Kim, K., 2010. A study on the grid-to-rod fretting wear-induced fuel failure observed in the 16X16KOFA fuel. Nucl. Eng. Des. 240, 756–762. doi:10.1016/j.nucengdes.2009.12.014

[35]   Kim, K., 2009. The study on grid-to-rod fretting wear models for PWR fuel. Nucl. Eng. Des. 239, 2820–2824. doi:10.1016/j.nucengdes.2009.08.018

[36]   Kim, K., Suh, J., 2009. Impact of Nuclear Fuel Assembly Design on Grid-to-Rod Fretting Wear. J. Nucl. Sci. Technol. 46, 149–157. doi:10.1080/18811248.2007.9711516

[37]   Kimura, N., Kamide, H., Emonot, P., Nagasawa, K., 2007a. Study on Thermal Striping Phenomena in Triple-Parallel Jet - Investigation on Non-Stationary Heat Transfer Characteristics Based on Numerical Simulation -, in: The 12th International Topical Meeting on Nuclear Reactor Thermal Hydraulics (NURETH-12). Pittsburgh, PA.

[38]   Kimura, N., Miyakoshi, H., Kamide, H., 2007b. Experimental investigation on transfer characteristics of temperature fluctuation from liquid sodium to wall in parallel triple-jet. Int. J. Heat Mass Transf. 50, 2024–2036. doi:10.1016/j.ijheatmasstransfer.2006.09.030

[39]   Kimura, N., Nishimura, M., Hayashi, K., Kamide, H., 1999. an Investigation of Thermal Stratification - Sodium Experiments and Analyses - 1–10.

[40]   Kimura, N., Nishimura, M., Kamide, H., 2002. Study on Convective Mixing for Thermal Striping Phenomena (Experimental Analyses on Mixing Process in Parallel Triple-Jet and Comparisons Between Numerical Methods). JSME Int. J. Ser. B. doi:10.1299/jsmeb.45.592

[41]   Kobayashi, J., Kimura, N., Tobita, A., Kamide, H., Watanabe, O., Ohyama, K., 2014. Study on Thermal Striping at UIS of Advanced Loop Type Fast Reactor, in: Proceedings of the 17th International Conference on Nuclear Engineering ICONE17. pp. 1–10.

[42]   Launder, B., Spalding, D., 1974. The Numerical Computation of Turbulent Flows. Comput. Methods Appl. Mech. Eng. 3, 269–289.

[43]   Launder, B.E., Reece, G.J., Rodi, W., 1975. Progress in the development of a Reynolds-stress turbulence closure. J. Fluid Mech. 537–566.

[44]   Lee, C.M., Choi, Y.D., 2007. Comparison of thermo-hydraulic performances of large scale vortex flow (LSVF) and small scale vortex flow (SSVF) mixing vanes in 17 x 17 nuclear rod bundle. Nucl. Eng. Des. 237, 2322–2331. doi:10.1016/j.nucengdes.2007.04.011

[45]   Lee, J.I., Hu, L.W., Saha, P., Kazimi, M., 2009. Numerical Analysis of Thermal Striping Induced High Cycle Thermal Fatigue in a Mixing Tee. Nucl. Eng. Des. 239, 833–839. doi:10.1016/j.nucengdes.2008.06.014

[46]   Lenci, G., 2016. A structure-resolving hybrid turbulence closure. Massachusetts Institute of Science and Technology.

[47]   Lesieur, M., Mankbadi, R.R., 1988. Turbulence in Fluids. J. Appl. Mech.

[48]   Liu, Z.G., Liu, Y., Lu, J., 2013. Numerical simulation of the fluid-structure interaction for two simple fuel assemblies. Nucl. Eng. Des. 258, 1–12. doi:10.1016/j.nucengdes.2013.01.029

[49]   Lomperski, S., Merzari, E., Obabko, A., Pointer, W.D., Fischer, P., 2012. The MAX Facility for CFD Code Validation, in: Proceedings of ICAPP 2012. Chicago, IL, pp. 1873–1879.

[50]   Lomperski, S., Pointer, D., Wiedmeyer, S., Fischer, P., Obabko, A., 2009. Multi-Dimensional Turbulent Gas Mixing Experiment (MAX) Design Report.

[51]   Lomperski, S., Pointer, D.W., 2015. MAX CFD Validation Data Set for Twin Isothermal Jets Nuclear Engineering Division. Nucl. Eng. Div. Argonne Natl. Lab.

[52]   Lu, D., Cao, Q., Lv, J., Xiao, Y., 2012. Experimental Study on Three-Dimensional Temperature Fluctuation Caused by Coaxial-Jet Flows. Nucl. Eng. Des. 243, 234–242. doi:10.1016/j.nucengdes.2011.11.017

[53]   Lu, R.Y., Karoutas, Z., Sham, T.L., 2011. CASL virtual reactor predictive simulation: Grid-to-Rod Fretting wear. Jom 63, 53–58. doi:10.1007/s11837-011-0139-6

[54]   Menter, F.R., Kuntz, M., Bender, R., 2003. A scale-adaptive simulation model for turbulent flow predictions. 41st Aerosp. Sci. Meet. Exhib. 1–11.

[55]   Merzari, E., Khakim, A., Ninokata, H., Baglietto, E., 2009. Unsteady Reynolds-averaged Navier-Stokes: toward accurate prediction of turbulent mixing phenomena. Int. J. Process Syst. Eng. 1, 100. doi:10.1504/IJPSE.2009.028003

[56]   Merzari, E., Pointer, W.D., Obabko, a, Fischer, P., 2010. On the Numerical Simulation of Thermal Striping in the Upper Plenum of a Fast Reactor. Proc. ICAPP 2010.

[57]   Moriya, S., Ohshima, I., 1990. Hydraulic Similarity in the Temperature Fluctuation Phenomena of Non-Isothermal Coaxial Jets. Nucl. Eng. Des. 120, 385–393. doi:10.1016/0029-5493(90)90388-E

[58]   Moriya, S., Ushijima, S., Tanaka, N., 1991. Thermal Striping Evaluation at Core Outlet by Seven-Assembly Water Model Test, in: Transactions of the 11th International Conference on Structural Mechanics in Reactor Technology.

[59]   Nicoud, F., Ducros, F., 1999. Subgrid-Scale Stress Modelling Based on the Square of the

Velocity Gradient Tensor 183–200.

[60]   Nishimura, M., Kimura, N., 2003. URANS Computations for an Oscillatory Non-Isothermal Triple-Jet Using the k-ε and Second Moment Closure Turbulence Models. Int. J. Numer. Methods Fluids 43, 1019–1044. doi:10.1002/fld.510

[61]   Nishimura, M., Tokuhiro, A., Kimura, N., Kamide, H., 2000. Numerical Study on Mixing of Oscillating Quasi-Planar Jets with Low Reynolds Number Turbulent Stress and Heat Flux Equation Models. Nucl. Eng. Des. 202, 77–95. doi:10.1016/S0029-5493(00)00287-9

[62]   Ohira, H., Honda, K., Sotsu, M., 2013. Numerical Simulations of Upper Plenum Thermal-Hydraulics of Monju Reactor Vessel Using High Resolution Mesh Models 7, 679–688.

[63]   Okui, S., Kubo, Y., Katinoki, S., Lu, R., Karoutas, Z., 2013. Flow-Induced Grid-to-Rod Fretting Test and Simulation for NFI PWR Fuel Assembly, in: Proceedings of the 2013 21st International Conference on Nuclear Engineering.

[64]   Omotowa, O., Skifton, R., Tokuhiro, A., 2012. Benchmark Studies of Thermal Jet Mixing in SFRs Using a Two-Jet Model, in: Proceedings of ICAPP 2012. Chicago, IL, pp. 2296–2301.

[65]   Peniguel, C., Sakiz, M., Benhamadouche, S., Stephan, J., Vindeirinho, C., 2003. Presentation of a Numerical 3D Approach to Tackle Thermal Striping in a PWR Nuclear T-Junction, in: Proceedings of the 2003 ASME Pressure Vessels and Piping Conference. Cleveland, OH, pp. 1–8.

[66]   Pointer, W.D., Lomperski, S., Fischer, P., Obabko, A., 2009. Proposed Experiment for Validation of Cfd Methods for Advanced Sfr Design: Upper Plenum Thermal Striping and Stratification. Proc. 17th Int. Conf. Nucl. Eng. ICONE17 1–13. doi:10.1115/ICONE17-75740

[67]   Pope, S.B., 2001. Turbulent Flows. Meas. Sci. Technol. 12, 2020–2021. doi:10.1088/0957-0233/12/11/705

[68]   Shih, T., Zhu, J., Lumley, J., 1995. A New Reynolds Stress Algebraic Equation Model. Comput. Methods Appl. Mech. Eng.

[69]   Tenchine, D., Moro, J.P., 1997. Experimental and Numerical Study of Coaxial Jets, in: Eight International Topical Meeting on Nuclear Reactor Thermal-Hydraulics. Kyoto, Japan.

[70]   Tenchine, D., Nam, H.Y., 1987. Thermal Hydraulics of Coaxial Sodium Jets. AiChE Symp. Ser. 83, 151–156.

[71]   Tokuhiro, A., Kimura, N., 1999. An Experimental Investigation on Thermal Striping. Mixing Phenomena of a Vertical Non-Buoyant Jet with Two Adjacent Buoyant Jets as Measured by Ultrasound Doppler Velocimetry. Nucl. Eng. Des. 188, 49–73. doi:10.1016/S0029-5493(99)00006-0

[72]   Ushijima, S., Tanaka, N., Moriya, S., 1990. Turbulence measurements and calculations of non-isothermal coaxial jets. Nucl. Eng. Des. 122, 85–94.

[73]   van den Berg, J.C., 2004. Wavelets in Physics.

[74]   Wakamatsu, M., Nei, H., Hashiguchi, K., 1995. Attenuation of Temperature Fluctuations in Thermal Striping. J. Nucl. Sci. Technol. 32, 752–762. doi:10.1080/18811248.1995.9731770

[75]   Wang, H., Lee, S., Hassan, Y.A., Ruggles, A.E., 2016. Laser-Doppler measurements of the turbulent mixing of two rectangular water jets impinging on a stationary pool. Int. J. Heat Mass Transf. 92, 206–227. doi:10.1016/j.ijheatmasstransfer.2015.08.084

[76]   Wille, R., Fernholz, H., 1965. Report on the first European Mechanics Colloquium, on the Coanda effect.

[77]   Xiang-bin, L., Dao-gang, L., Cao, Q., 2012. Analysis of Coolant Temperature Fluctuating in Upper Plenum of PWR. At. Energy Sci. Technol.

[78]   Yan, J., Yuan, K., Tatli, E., Karoutas, Z., 2011. A new method to predict Grid-To-Rod Fretting in a PWR fuel assembly inlet region. Nucl. Eng. Des. 241, 2974–2982.

doi:10.1016/j.nucengdes.2011.06.019

[79] Yuki, K., Hashizume, H., Tanaka, M., Muramatsu, T., 2006. Investigation of Thermal Hydraulic Mixing Mechanism in T-junction Pipe with a 90-degree Bend in Upstream Side for Mitigation and Controlling of Thermal-striping Phenomena.